NASA TECHNICAL
MEMORANDUM

NASA TM X-64779

SIMULATION OF AN EXPERIMENT POINTING SYSTEM FOR THE SPACE SHUTTLE

By P. D. Nicaise
Preliminary Design Office
Program Development

September 1973

NASA

George C. Marshall Space Flight Center
Marshall Space Flight Center, Alabama

1. REPORT NO. NASA TM X-64779	2. GOVERNMENT ACCESSION NO.	3. RECIPIENT'S CATALOG NO.
4. TITLE AND SUBTITLE Simulation of an Experiment Pointing System for the Space Shuttle		5. REPORT DATE September 1973
		6. PERFORMING ORGANIZATION CODE PD-DO-E
7. AUTHOR(S) P. D. Nicaise		8. PERFORMING ORGANIZATION REPORT #
9. PERFORMING ORGANIZATION NAME AND ADDRESS George C. Marshall Space Flight Center Marshall Space Flight Center, Alabama 35812		10. WORK UNIT NO.
		11. CONTRACT OR GRANT NO.
		13. TYPE OF REPORT & PERIOD COVERED
12. SPONSORING AGENCY NAME AND ADDRESS National Aeronautics and Space Administration Washington, D.C. 20546		Technical Memorandum
		14. SPONSORING AGENCY CODE

15. SUPPLEMENTARY NOTES

16. ABSTRACT

The pointing and control of experiments during sortie missions are examined from the standpoint of accuracy and performance. The effect of gimbal characteristics, pallet stiffness, and variation in the servo control loop are described. Simulation results are shown for a number of pointing options under the disturbing influences of man motion, thruster firings, and experiment operations. One option of particular interest is the suspended pallet which offers the possibility of high accuracy pointing of very large payloads without using conventional gimbals. The pallet is suspended within the payload bay by non-rigid attachments such as springs, thereby isolating experiments from most Shuttle disturbances. Control moment gyros apply torques directly to the pallet to maintain pointing accuracy within the arc second range. Spring torques constrain Shuttle attitude so thruster operation is not required. The suspended pallet approach will meet the base stability requirements of any sortie experiment and offers the possibility of a standardized low weight, low cost alternative to gimbaled mounts. However, the practical aspects, including possible implementation problems, have not been fully explored.

17. KEY WORDS Space Shuttle Pointing and Control Sortie Experiment Stabilization Standardized Experiment Mounts Experiment Pointing Accuracy Simulation of Experiment Disturbances Spacelab Experiment Pointing Problems	18. DISTRIBUTION STATEMENT Unclassified-unlimited *William R. Marshu* ERICH E. GOERNER Director, Preliminary Design Office

19. SECURITY CLASSIF. (of this report) Unclassified	20. SECURITY CLASSIF. (of this page) Unclassified	21. NO. OF PAGES 54	22. PRICE NTIS

ACKNOWLEDGEMENTS

TABLE OF CONTENTS

DEFINITION OF SYMBOLS

a_0	Thruster position control gain
a_1	Thruster rate control gain
A_0	CMG position control gain
A_1	CMG rate control gain
d	Offset between the SEM gimbal axis and experiment CM
D_p	Pallet damping coefficient
F_A	Forces at pallet/Shuttle attach point
F_G	Forces at SEM gimbal point
I_E	Inertia of the experiment package
I_P	Inertia of the pallet
I_S	Inertia of the Shuttle
k_0	SEM position control gain
k_1	SEM rate control gain
k_{-1}	SEM integral control gain
K_A	Amplifier gain
K_E	Spring constant on SEM
K_M	Motor gain
K_P	Spring constant on the pallet
$\mathcal{L}$	The Lagrangian function
ℓ	Distance from Shuttle CM to pallet attach point
L	Distance from Shuttle/pallet attach point to gimbal axis
M_E	Mass of experiment package
M_P	Mass of pallet plus SEM
r	Distance from pallet CM to Shuttle/pallet attach point
R	Distance from pallet CM to gimbal axis
S	Laplace operator
X_E	Displacement of experiment CM
X_P	Displacement of pallet CM
Z_E	Displacement of experiment CM
Z_P	Displacement of pallet CM

DEFINITION OF SYMBOLS (CONCLUDED)

α	Angle between Shuttle and pallet
β	Angle between pallet and SEM
θ	Angle of SEM relative to inertial axes
ρ	Angle of pallet relative to inertial axes
τ	Time constant
φ	Angle of Shuttle relative to inertial axes

DEFINITION OF ACRONYMS

CG	Center of gravity
CM	Center of mass
CMG	Control moment gyro
DB	Deadband
DIF	Logic Differentiator
EAI	Electronics Associates Inc.
EPS	Experiment pointing system (Skylab)
IC	Initial condition mode (analog computer)
LIM	Limit
NAR	North American Rockwell
OP	Operate mode (analog computer)
RCS	Reaction control system
RF	Rolling friction
SEM	Standardized experiment mount

SPAR MOUNTED TELESCOPES

PHOTOHELIOGRAPH

SORTIE LAB

SOLAR OBSERVATORY
SPACE SHUTTLE SORTIE MISSION

MARSHALL SPACE FLIGHT CENTER
MSFC-72-PD-4000-400

SIMULATION OF AN EXPERIMENT POINTING SYSTEM FOR THE SPACE SHUTTLE

INTRODUCTION

The Space Shuttle was originally conceived as a transport vehicle to ferry men and equipment into orbit and return them to a convenient landing site on the earth. It now appears likely that the Shuttle must also fill the role of a temporary orbital station during the interval between the Skylab mission and the establishment of a permanent Space Station. This role becomes even more important as the prospects for a permanent Space Station continue to recede. If there are to be any man-tended, gravity-free research or observations from space for many years after Skylab, they will almost certainly be carried out on the Shuttle during a Sortie mission. The Shuttle is expected to fulfill this role by carrying an inhabitable laboratory in the payload bay and maintaining a relatively stable attitude in orbit for at least several days. A variety of scientific experiments, including observations of the earth and other celestial objects, could be made from this laboratory.

A significant concern about the Sortie mission is the level of stability that can reasonably be maintained for the Shuttle, and even more important is what pointing accuracy can be expected for the experiments. These general questions were examined and much of the background for the current study is given in a previous report (Reference 1). The referenced report described the Phase B Orbiter stability characteristics and proposed some improvements for the experiment pointing mode. A Standardized Experiment Mount (SEM), which is Sortie Lab common ancillary equipment, was recommended for experiments with highly accurate pointing requirements. The SEM was visualized as a universal mount that could replace all specialized mounts and accommodate a wide variety of experiments. One or two SEMs could be mounted in the payload bay to point large telescopes or a number of smaller experiments. The current pressure to standardize and provide payload accommodation at minimum cost makes the SEM an especially attractive option.

This report presents the results of an in-house simulation study of the general pointing problems during a Sortie mission with special emphasis on SEM performance. An alternative to the SEM is examined which has high accuracy pointing capability and would probably be an even more economical approach than the SEM.

THE SIMULATION MODEL

The Shuttle, pallet, and SEM were considered to be three interacting bodies as shown in Figure 1. The equations were developed from this model and simplified to meet the requirements for the analog program. The equation development and simplification are described in Appendix A. Shuttle characteristics were taken from a North American Rockwell design as described in Reference 2. A summary of these characteristics and also those for the pallet and SEM is given in Table 1.

This program contains a number of options for making comparison studies. Shuttle control can be switched from thrusters to control moment gyros (CMGs). There is also an option for a flexible or rigid pallet structure. The following SEM bearing characteristics can be added individually or in combination: (1) Stiction (static friction), representative of preloaded ball bearings; (2) coulomb friction which can result from bearing motion, cable deformation, or hysteresis in the torquers; and (3) spring torques that result from flex pivots or cables. There is an option for adding an integral of position term to the SEM control loop. Any combination of gravity gradient, wall pushoff, random motion, and signal noise can be input as a disturbing function. The characteristics of the wall pushoff were taken from measurements made during a zero-gravity maneuver in a C-141 aircraft as described in Reference 3. The CMG and SEM control loops were modeled from Skylab CMG and experiment pointing system (EPS) characteristics that are summarized in Table 2.

A math flow diagram for this problem is shown in Figure 2. This diagram represents the equations of motion for the three bodies plus the control loops for the Shuttle and SEM. It defines the basic mathematical model which was programmed on an EAI 680 analog computer. It has been extensively verified and checked against analytical results. There are several features of this program which are not commonly used but appear to give good results for this

2

application. Appendix B shows some of these techniques which should be useful for developing similar programs.

SIMULATION RESULTS

A large amount of data has come from the simulation in the form of chart recordings. Samples of these recordings are shown in Appendix C. These data have application to a broad spectrum of questions concerning Shuttle stability, Shuttle/payload interface and experiment pointing accuracy. The general understanding and insight provided by the simulation is perhaps even more important than the data. Another valuable byproduct of this study is the highly refined and versatile analog program. This program will be maintained to answer specific questions that may arise in the future. It provides a means for rapid assessment of alternate hardware proposals and pointing techniques. A simulation, such as this one, provides the only means for resolving these questions because of the complex control problems and the nature of the disturbing functions.

The computer output is summarized here in the form of processed data that can be interpreted without a detailed understanding of the chart recordings. Figure 3 shows the relative contribution of each factor to experiment pointing error. Figure 4 shows the angular deviation and rate error that appears on the SEM as a result of thruster operation. This relationship assumes the Shuttle and SEM as defined in Table 2 with a completely rigid pallet. Figure 5 shows the amount of attenuation that is provided by a flexible pallet between the Shuttle and SEM. Figure 6 defines the SEM angular and rate error to be expected for various magnitudes of gimbal friction. This curve applies to either coulomb or static friction.

CONCLUSIONS

The stability of the SEM is limited primarily by the bearing characteristics and the interconnections across the gimbals. The disturbances such as thruster operation, man motion, gravity gradient torques, and signal noise are secondary influences. The stiction characteristics of conventional, large diameter bearings make them

3

unsuitable for an SEM stability requirement of 1 arc sec or less (Figure 3). This fact rules out the possibility of high accuracy pointing with wide angle capability in all three axes from a single gimbal design. However, for experiments which can tolerate momentary disturbances, the conventional gimbals could provide a practical mount. Constant limit cycle of the Shuttle is a preferable operating mode for a mount with conventional gimbal bearings. A dual or compound arrangement that permits large angular freedom by a conventional bearing plus a precision bearing which operates over a limited range appears to be the only choice for constant, high accuracy pointing. Even with the dual gimbal design, the center of mass (CM) of the experiment package must be maintained relatively close to the gimbal axes and coulomb friction of the precision bearing should be minimized. The flex pivot and gas bearing offer almost ideal characteristics and the gas bearing has a large angular range in one axis. Current estimates show that it would make an insignificant contribution to the contamination problem. The flex pivot can meet the performance requirements as shown by this study. However, its range is restricted to only a few degrees and it is very difficult to provide a flex pivot design for all three axes.

Pallet stiffness, within reasonable limits, presents no serious obstacle to SEM stability. In fact, a certain amount of "softness" in the structure attenuates short duration forces such as thruster firings. Intentional decoupling of the pallet from the Shuttle airframe by means of springs or other support devices results in a very promising pointing concept. High accuracy pointing can be achieved without an SEM by CMG stabilization of the pallet. There are no gimbal bearings and the entire pallet structure could serve as the experiment mount. The CMGs control the pallet and thereby indirectly control the Shuttle through the interconnecting springs. A conceptual drawing of such a configuration is shown in Figure 7. This "suspended pallet" concept may not quite match the precision of a torquer-controlled table because of CMG vibration or response characteristics. However, its obvious advantages in simplicity and low cost should warrant a more detailed investigation.

The current location of the Reaction Control System (RCS) modules near the Shuttle center line results in a much smaller angular impulse about the roll axis and better "balance" relative to the other axes. This condition is a great improvement over previous configurations and greatly reduces the case for low-level thrusters from the

standpoint of stability and pointing degradation. Of course contamination and propellant consumption, especially for continuous pointing with small deadbands, is still a problem. However, the large thrusters do not significantly degrade SEM operation and they can be operated in a "differential thrusting" mode to assure an efficient transfer to CMG control if necessary. Therefore, it appears that the large thruster versus low-level thruster question must be resolved on the basis of contamination, propellant consumption, and economy.

The stability levels which are described in this report for Shuttle attached pointing systems are obviously not as good as those obtained with free-flying spacecraft such as the Orbiting Astronomical Observatory (OAO). However, the advantages offered by the Sortie mission, namely manned access, avionics connections by hardwire, and direct attachment to the Shuttle are the very factors which limit experiment stability. Therefore, the environment may never be as clean, or the stability as precise as for free-flying spacecraft. However, this study has shown that state-of-the-art pointing systems can meet the requirements of all currently proposed Sortie experiments and almost certainly for many others that will appear in the future.

TABLE 1. SUMMARY OF SHUTTLE, PALLET, AND SEM CHARACTERISTICS

ITEM	MASS KG (LB)	INERTIA $N-M-S^2$ (SLUG FT^2)		
		I_{XX}	I_{YY}	I_{ZZ}
150K LB ORBITER (+25K LB PAYLOAD)	$87,868 \times 10^6$ ($193,717 \times 10^6$)	1.097×10^6 (0.809×10^6)	8.120×10^6 (5.989×10^6)	8.405×10^6 (6.199×10^6)
30–FT PALLET	1,578 (3,480)	– –	14,643 (10,800)	14,643 (10,800)
EXPERIMENT MOUNT	1,810 (4,000)	– –	– –	– –
EXPERIMENT PACKAGE	2,948 (6,500)	– –	4,108 (3,030)	4,108 (3,030)

TABLE 2. SUMMARY OF CMG AND EPS CHARACTERISTICS

CMG CHARACTERISTICS

O MOMENTUM CAPACITY: 3120 N-M-S (2300 FT–LB–S)/UNIT
O MAXIMUM TORQUE OUTPUT: 186 N–M (135 FT–LB)/UNIT
O TRANSFER FUNCTION: 30/(S+30)
O SYSTEM BANDWIDTH: 0.022 HZ

EPS CHARACTERISTICS

O MAXIMUM TORQUE OUTPUT: 9.5 N–M (7 FT–LB)/TORQUER
O COULOMB FRICTION LEVEL: 0.4 N–M(0.3 FT–LB)
O SPRING TORQUE: 0.54 M–N/DEG (0.4 FT–LB/DEG)
O SYSTEM BANDWIDTH: 2.3 HZ
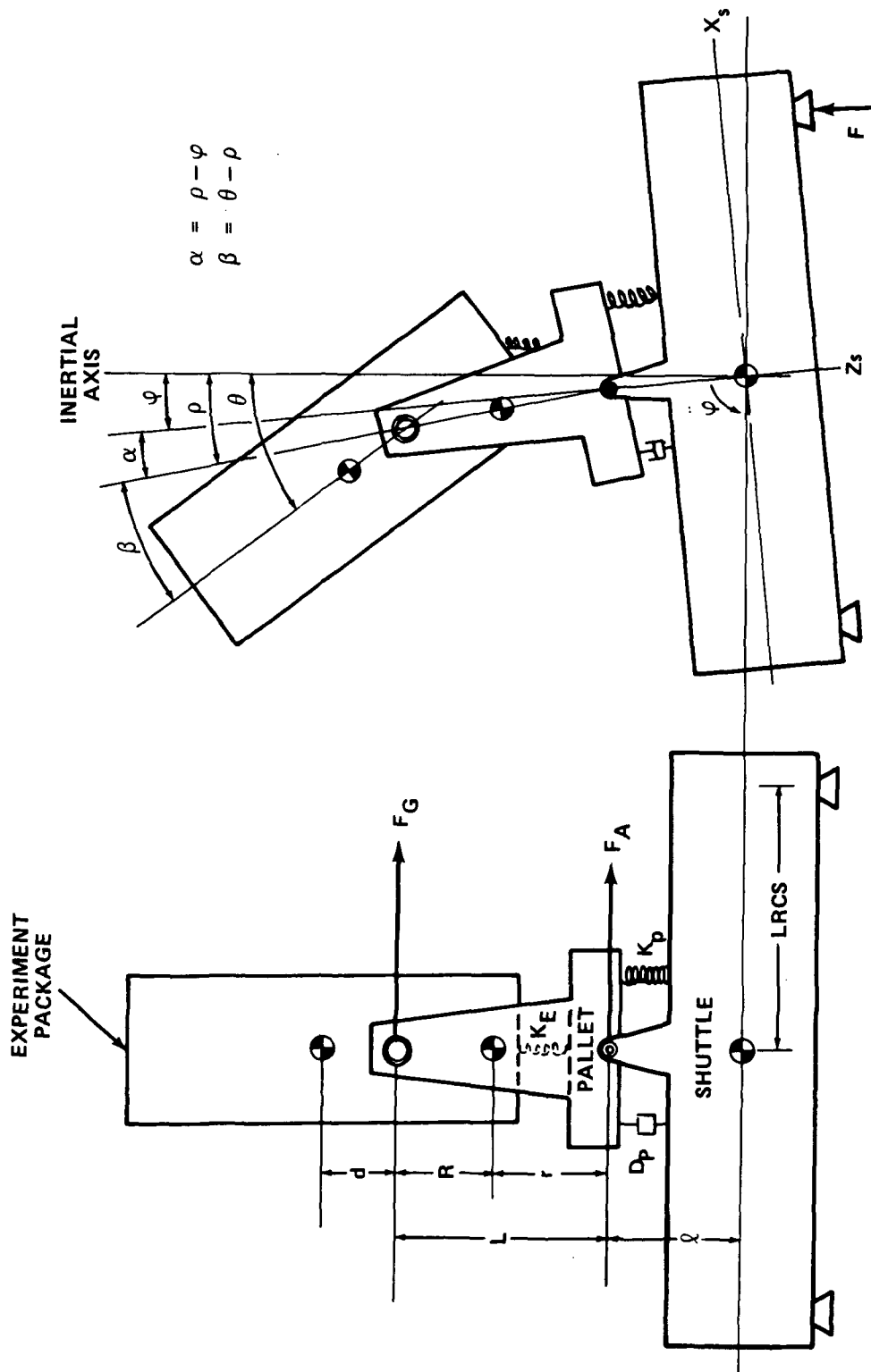
Figure 1. Dynamic model.

$\alpha = \rho - \varphi$

$\beta = \theta - \rho$
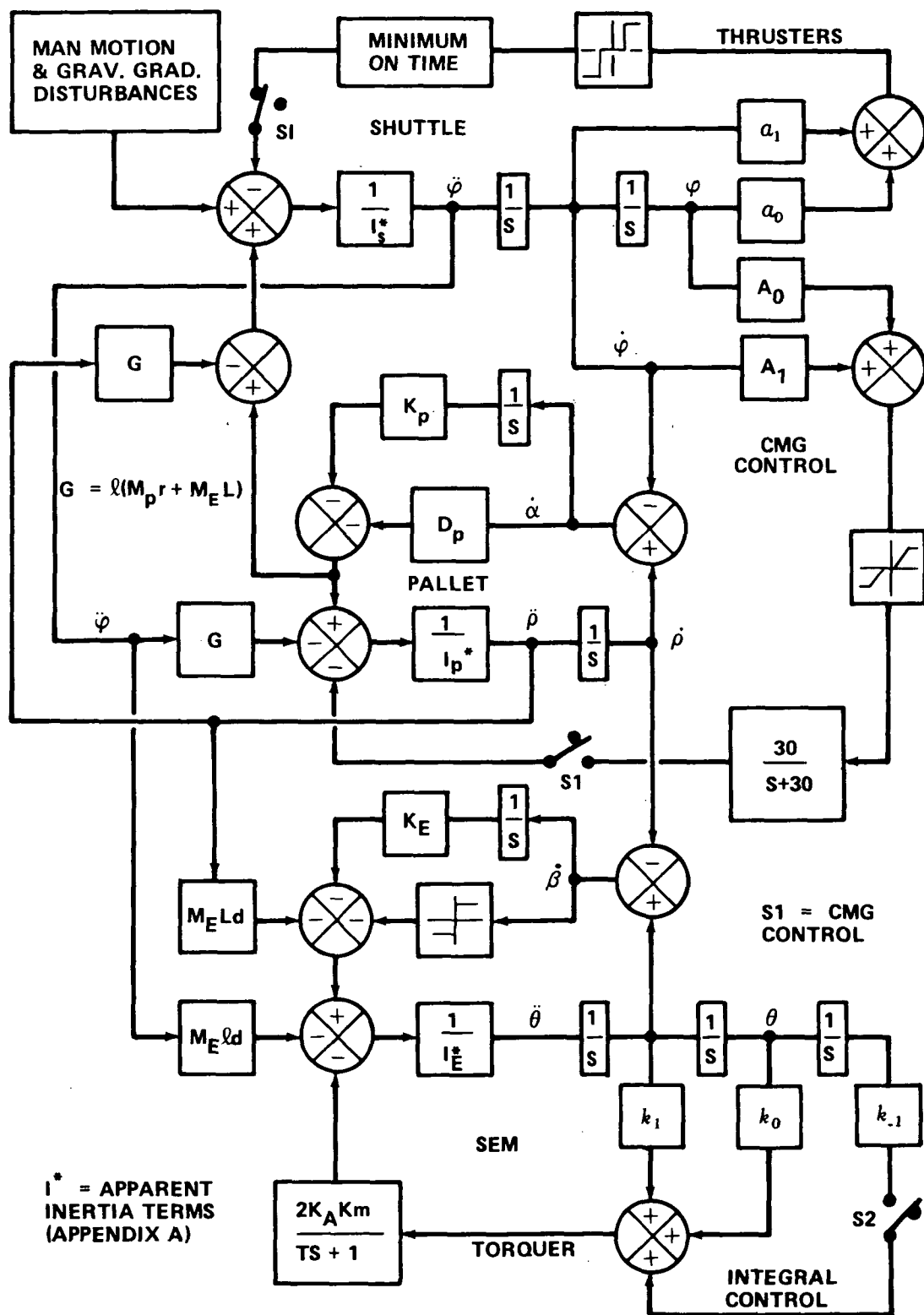
Figure 2. Mathematical flow diagram.
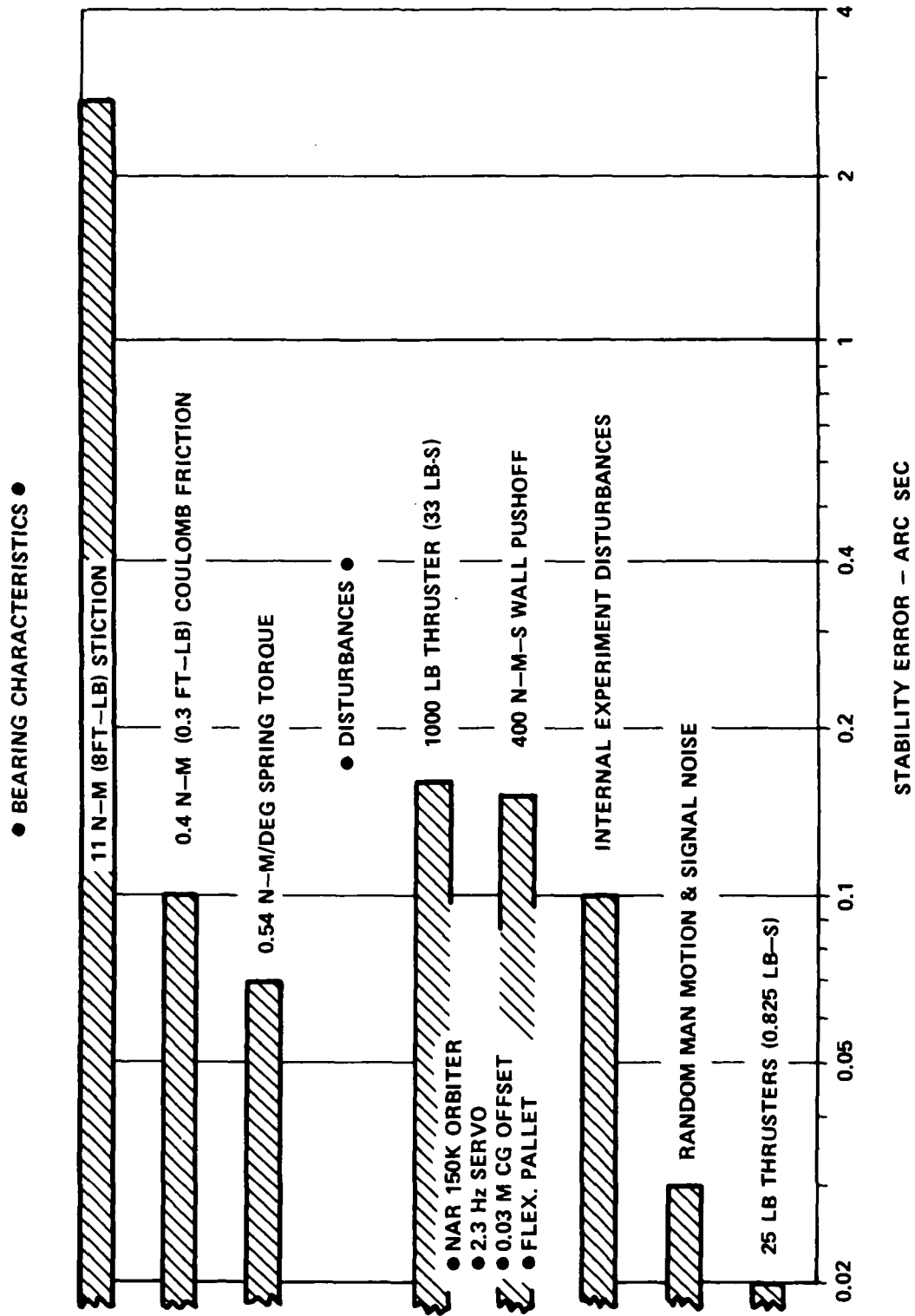
Figure 3. Contributors to experiment error.

9
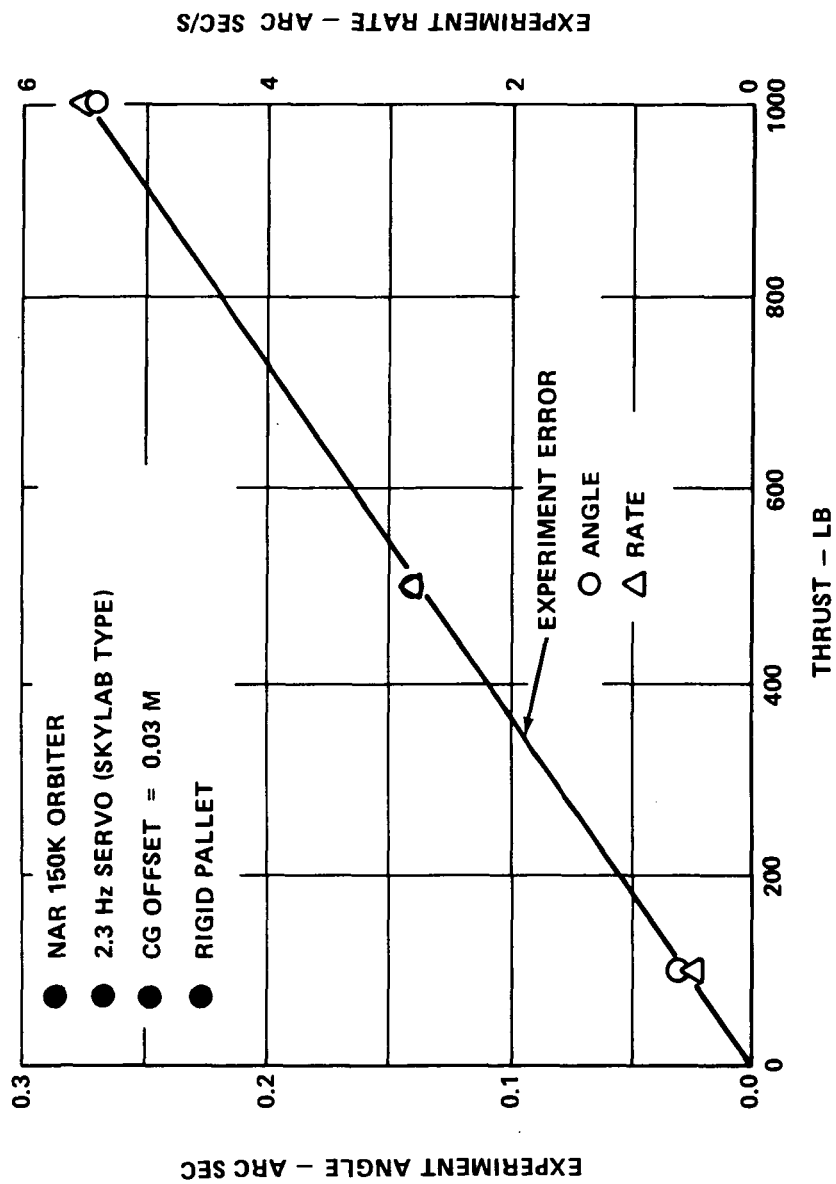
Figure 4. Sensitivity to thrust level.

10
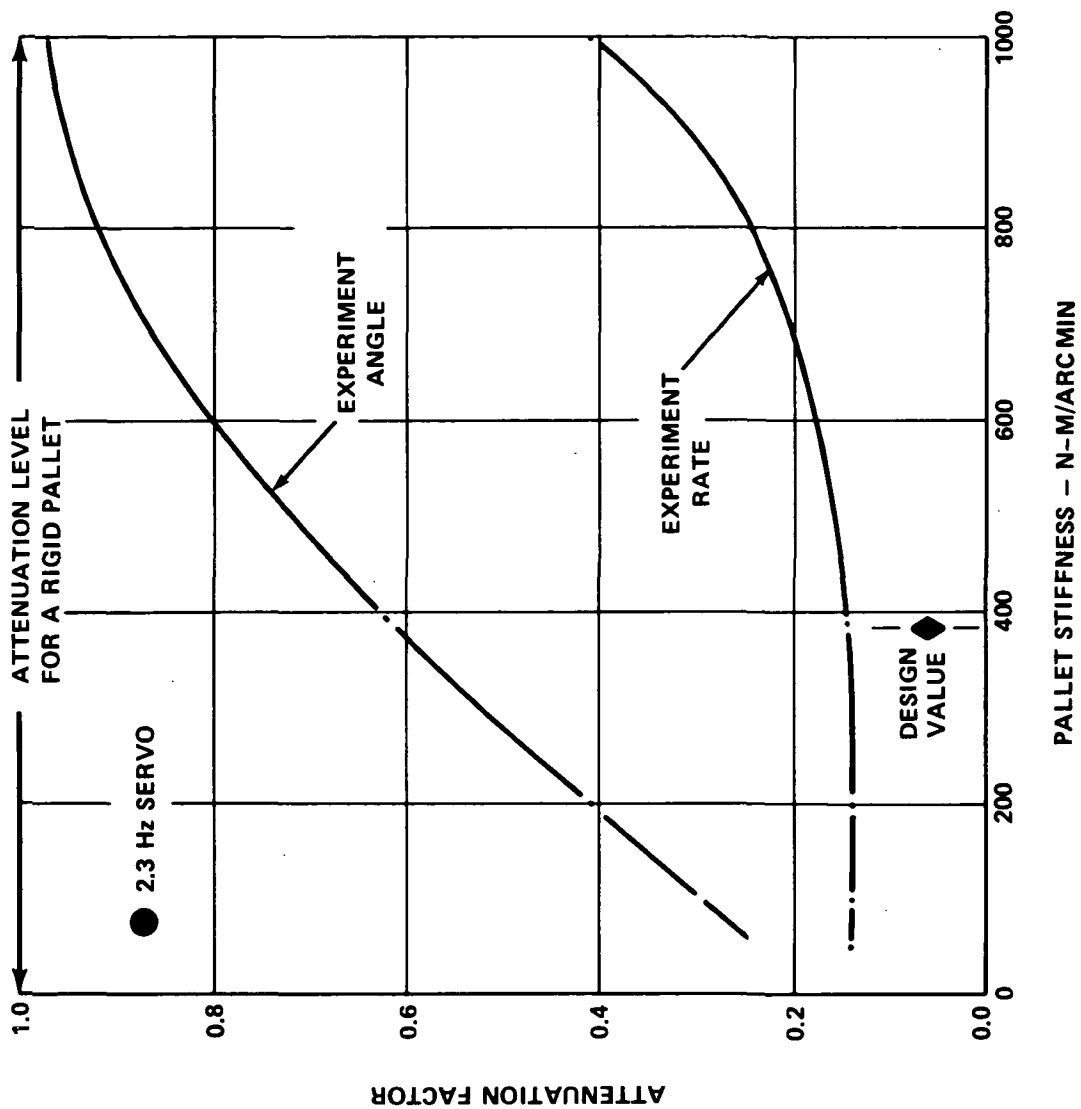
Figure 5. Pallet attenuation of thruster-induced disturbances.
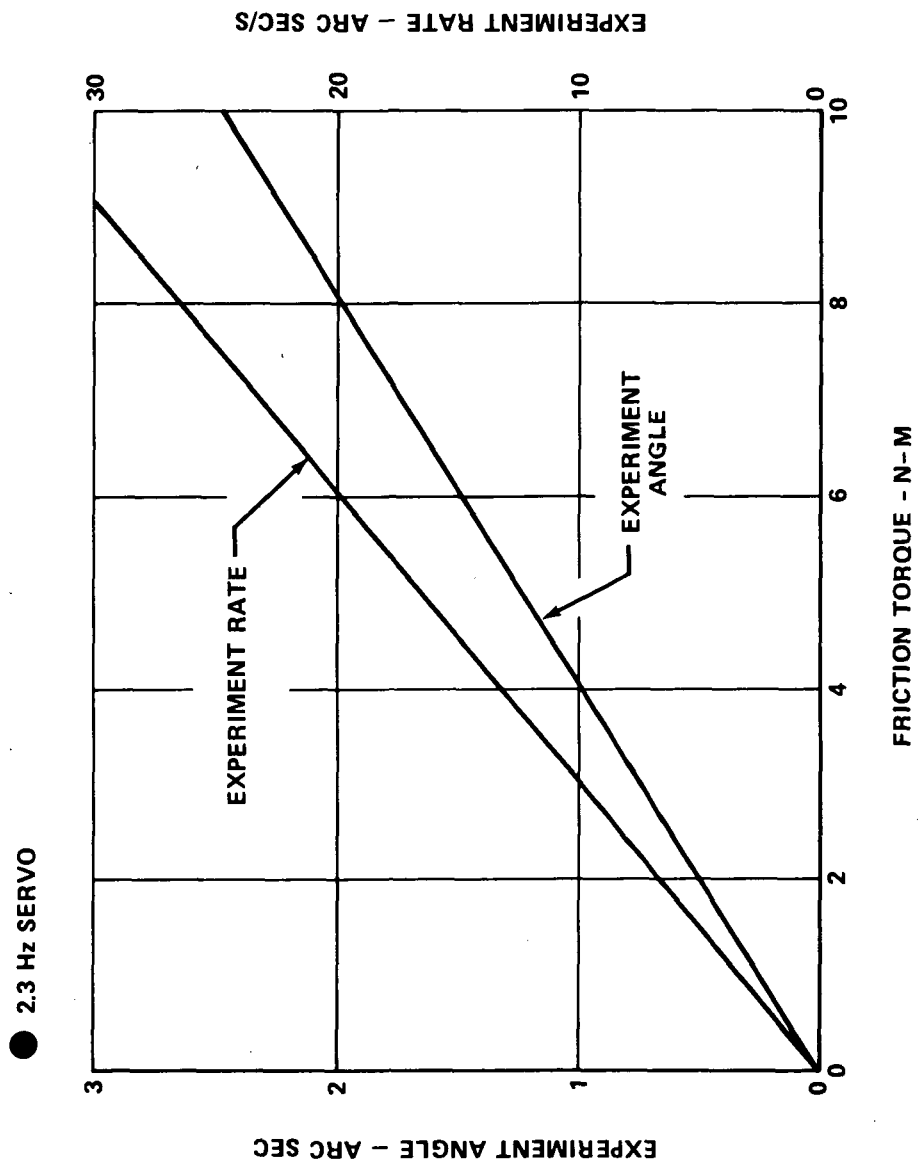
Figure 6. Sensitivity to gimbal friction.

THE SUSPENDED PALLET PROVIDES A
HIGH LEVEL OF STABILITY FOR A
WIDE VARIETY OF EXPERIMENTS

OFFSET OR COARSE
POINTING IS ACHIEVED
WITH POSITION & HOLD
MOUNTS.

SHOCK MOUNTED CMG'S APPLY TORQUE
DIRECTLY TO THE PALLET AND SHUTTLE
ORIENTATION IS MAINTAINED BY THE
INTERCONNECTING SUSPENSION DEVICES

SPRINGS OR OTHER NON-RIGID SUSPENSION DEVICES
ISOLATE THE PALLET FROM SHUTTLE DISTURBANCES
SUCH AS MAN MOTION.

● OTHER FEATURES:

● NO RCS REQUIRED
● FULL SKY COVERAGE
● LOW WEIGHT
● LARGE MOUNTING
  SURFACE
● MINIMUM PALLET/
  SHUTTLE INTERFACE
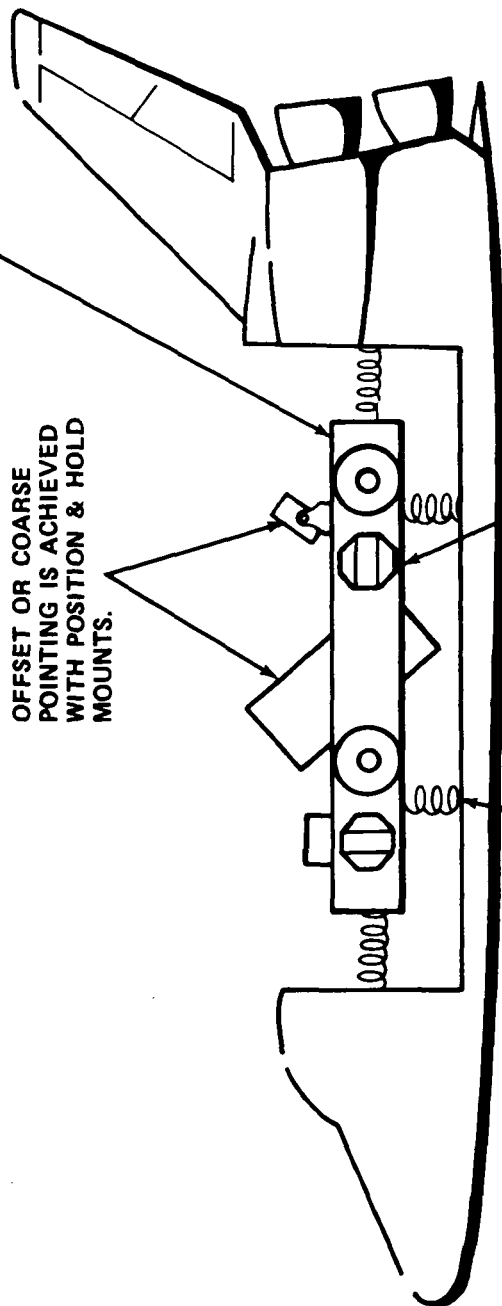
Figure 7.   Conceptual drawing of the suspended pallet.

13

APPENDIX A
EQUATION DEVELOPMENT

In developing the equations of motion for this restricted, three-body problem Lagrangian dynamics were applied to the bodies with the following simplifying conditions: (1) All motion was limited to a plane, and (2) translation of the Shuttle was neglected. These assumptions and others that will appear later in the development have been shown to be valid for this problem.

Consider the model as defined by Figure 1. The geometric and dynamic relationships for the three bodies are as follows:

$$X_p = X_s - \ell \sin \varphi - r \sin \rho \tag{1}$$

$$\dot{X}_p = \dot{X}_s - \ell \dot{\varphi} \cos \varphi - r \dot{\rho} \cos \rho \tag{2}$$

$$\ddot{X}_p = \ddot{X}_s - \ell (\ddot{\varphi} \cos \varphi - \dot{\varphi}^2 \sin \varphi) - r (\ddot{\rho} \cos \rho - \dot{\rho}^2 \sin \rho) \tag{3}$$

$$Z_p = Z_s - \ell \cos \varphi - r \cos \rho \tag{4}$$

$$\dot{Z}_p = \dot{Z}_s + \ell \dot{\varphi} \sin \varphi + r \dot{\rho} \sin \varphi \tag{5}$$

$$\ddot{Z}_p = \ddot{Z}_s + \ell (\ddot{\varphi} \sin \varphi + \dot{\varphi}^2 \cos \varphi) + r (\ddot{\rho} \sin \varphi + \dot{\rho}^2 \cos \rho) \tag{6}$$

$$X_E = X_p - R \sin \rho - d \sin \theta \tag{7}$$

$$\dot{X}_E = \dot{X}_p - R \dot{\rho} \cos \rho - d \dot{\theta} \cos \theta \tag{8}$$

$$\ddot{X}_E = \ddot{X}_p - R (\ddot{\rho} \cos \rho - \dot{\rho}^2 \sin \rho) - d (\ddot{\theta} \cos \theta - \dot{\theta}^2 \sin \theta) \tag{9}$$

$$Z_E = Z_p - R \cos \rho - d \cos \theta \tag{10}$$

$$\dot{Z}_E = \dot{Z}_p + R \dot{\rho} \sin \rho + d \dot{\theta} \sin \theta \tag{11}$$

$$\ddot{Z}_E = \ddot{Z}_p + R (\ddot{\rho} \sin \rho + \dot{\rho}^2 \cos \rho) + d (\ddot{\theta} \sin \theta + \dot{\theta}^2 \cos \theta) \tag{12}$$

The kinetic energy equation is

$$T = \tfrac{1}{2}M \sin (\dot{X}_s^2 + \dot{Z}_s^2) + \tfrac{1}{2}M_p (\dot{X}_p^2 + \dot{Z}_p^2) + \tfrac{1}{2}M_E(\dot{X}_E^2 + \dot{Z}_E^2) \quad (13)$$

The potential energy equation is

$$V = \tfrac{1}{2}K_p\alpha^2 + \tfrac{1}{2}K_E\beta^2 \quad , \quad \alpha = \rho - \varphi , \quad \beta = \theta - \rho \quad\quad (14)$$

Following is Lagrange's equation:

$$F_{qi} = \frac{d}{dt} (\frac{\delta \mathcal{L}}{\delta qi}) - \frac{\delta \mathcal{L}}{\delta qi} \quad , \quad \mathcal{L} = T - V \quad\quad (15)$$

The following terms are derived for Lagrange's equation:

$$\frac{\delta \mathcal{L}}{\delta \theta} = M_E d\dot{\theta} (\dot{X}_E \sin \theta + \dot{Z}_E \cos \theta) - K_E\beta \quad\quad (16)$$

$$\frac{\delta \mathcal{L}}{\delta \rho} = M_p r\dot{\rho} (\dot{X}_p \sin \rho + \dot{Z}\rho \cos \rho)$$

$$+ M_E \dot{\rho}L (\dot{X}_E \sin \rho + \dot{Z}_E \cos \rho) - K_p\alpha + K_E\beta \quad\quad (17)$$

$$\frac{\delta \mathcal{L}}{\delta \varphi} = \ell \dot{\varphi}[M_p (\dot{X}_p \sin \varphi + \dot{Z}_p \cos \varphi) + M_E (\dot{X}_E \sin \varphi$$

$$+ \dot{Z}_E \cos \varphi)] + K_p (\rho - \varphi) \quad\quad (18)$$

$$\frac{d}{dt} (\frac{\delta \mathcal{L}}{\delta \dot{\theta}}) = I_E\ddot{\theta} - M_E d (\ddot{X}_E \cos \theta - \ddot{Z}_E \sin \theta - \dot{X}_E\dot{\theta} \sin \theta$$

$$- \ddot{Z}_E\dot{\theta} \cos \theta) \quad\quad (19)$$

16

$$\frac{d}{dt}\frac{\delta \mathcal{L}}{\delta \dot{\rho}} = I_p\ddot{\rho} - M_p r \,(\ddot{X}_p \cos \rho - \dot{X}_p \dot{\rho} \sin \rho - \ddot{Z}_p \sin \rho$$

$$- \dot{Z}_p \dot{\rho} \cos \rho) - M_E L \,(\ddot{X}_E \cos \varphi - \dot{X}_E \dot{\rho} \sin \rho \qquad (20)$$

$$- \ddot{Z}_E \sin \rho - \dot{Z}_E \dot{\rho} \cos \rho)$$

$$\frac{d}{dt}\frac{\delta \mathcal{L}}{\delta \dot{\varphi}} = I_s\ddot{\varphi} - M_p \ell \,(\ddot{X}_p \cos \varphi - \dot{X}_p \dot{\varphi} \sin \varphi - \ddot{Z}_p \sin \varphi$$

$$- \dot{Z}_p \dot{\varphi} \cos \varphi) - M_E \ell \,(\ddot{X}_E \cos \varphi - \dot{X}_E \dot{\varphi} \sin \varphi \qquad (21)$$

$$- \ddot{Z}_E \sin \varphi - \dot{Z}_E \dot{\varphi} \cos \varphi)$$

The rotational equations of motion are obtained from Lagrange's equation:

$$F_\theta = \Sigma T_E = I_E\ddot{\theta} - M_E d \,(\ddot{X}_E \cos \theta - \ddot{Z}_E \sin \theta) + K_E \beta \qquad (22)$$

$$F_p = \Sigma T_p = I_p\ddot{\rho} - M_p r \,(\ddot{X}_p \cos \rho - \ddot{Z}_E \sin \rho)$$

$$- M_E L \,(\ddot{X}_E \cos \rho - \ddot{Z}_E \sin \rho) + K_p \alpha + D_p \dot{\alpha} - K_E \beta \qquad (23)$$

$$F_\varphi = \Sigma T_s = I_s\ddot{\varphi} - M_p \ell \,(\ddot{X}_p \cos \varphi - \ddot{Z}_p \sin \varphi)$$

$$- M_E \ell \,(\ddot{X}_E \cos \varphi - \ddot{Z}_E \sin \varphi) - K_p \alpha - D_p A \qquad (24)$$

These equations are simplified by making small angle approximations and neglecting Shuttle translational terms. Equations (3), (6), (9), and (12) are substituted into equations (22), (23), and (24). The terms are rearranged for convenient analog programming.

$$(I_E + M_E d^2)\,\ddot{\theta} = -(M_E \ell d)\,\ddot{\varphi} - (M_E Ld)\,\ddot{\rho} - K_E \beta + \Sigma T_E \qquad (25)$$

$$(I_p + M_p r^2 + M_E L^2)\,\ddot{\rho} = -(M_p r\ell + M_E L\ell)\,\ddot{\varphi} - (M_E Ld)\,\ddot{\theta}$$

$$(26)$$

$$- K_p \alpha - D_p \dot{\alpha} + K_E \beta + \Sigma T_p$$

$$(I_s + M_p \ell^2 + M_E \ell^2) \ddot{\varphi} = - (M_p r\ell + M_E L\ell) \ddot{\rho} - (M_E \ell d) \ddot{\theta}$$

$$+ K_p \alpha + D_p \dot{\alpha} + \Sigma T_s \tag{27}$$

Equations (25, (26), and (27) form the basis for that part of the program which describes the dynamics of the three hinged bodies. The $(M_E \ell d) \dot{\theta}$ terms and the $K_E \beta$ term of equation (26) were found to have a negligible effect on the analog output. The bracketed terms on the left sides of these equations represent "apparent" inertia of each body that results from the interconnections. The set of equations used for the block diagram in Figure 2 were obtained by redefining terms:

$$I_E^* \ddot{\theta} = - (M_E \ell d) \ddot{\varphi} - (M_E L d) \ddot{\rho} - K_E \beta + \Sigma T_E \tag{28}$$

$$I_p^* \ddot{\rho} = -G \ddot{\varphi} - (M_E L d) \ddot{\theta} - K_p \alpha - D_p \dot{\alpha} = K_E \beta + \Sigma T_p \tag{29}$$

$$I_s^* \ddot{\varphi} = -G \ddot{\rho} - (M_E \ell d) \ddot{\theta} + K_p \alpha + D_p \dot{\alpha} + \Sigma T_s \tag{30}$$

18

APPENDIX B

IMPLEMENTATION OF SPECIALIZED ANALOG FUNCTIONS

Figure B1 shows a method of simulating static and rolling friction between two bodies which are both rotating relative to inertial space. The rolling friction imposes a fixed torque level that is always in opposition to the direction of motion. Stiction is achieved by setting the $\dot\theta$ integrator to initial condition (IC) whenever relative rate goes through zero and driving $\dot\theta$ directly with the $\dot\rho$ signal. This results in a "hard" stiction which is removed only when torque level reaches the stiction limit.

Figure B2 is a simple relay implementation of the wall push-off function. It produces a close approximation to the expected disturbance with a minimum of machine components.

Figure B3 shows an implementation of thruster output which includes minimum on-time logic. The integrator timers were used instead of monostable timers to permit changes in time base from the keyboard without resetting the monostable period. This scheme produces near ideal pulses that may be filtered to approximate thrust buildup.

Figure B1. Static and rolling friction logic.

20
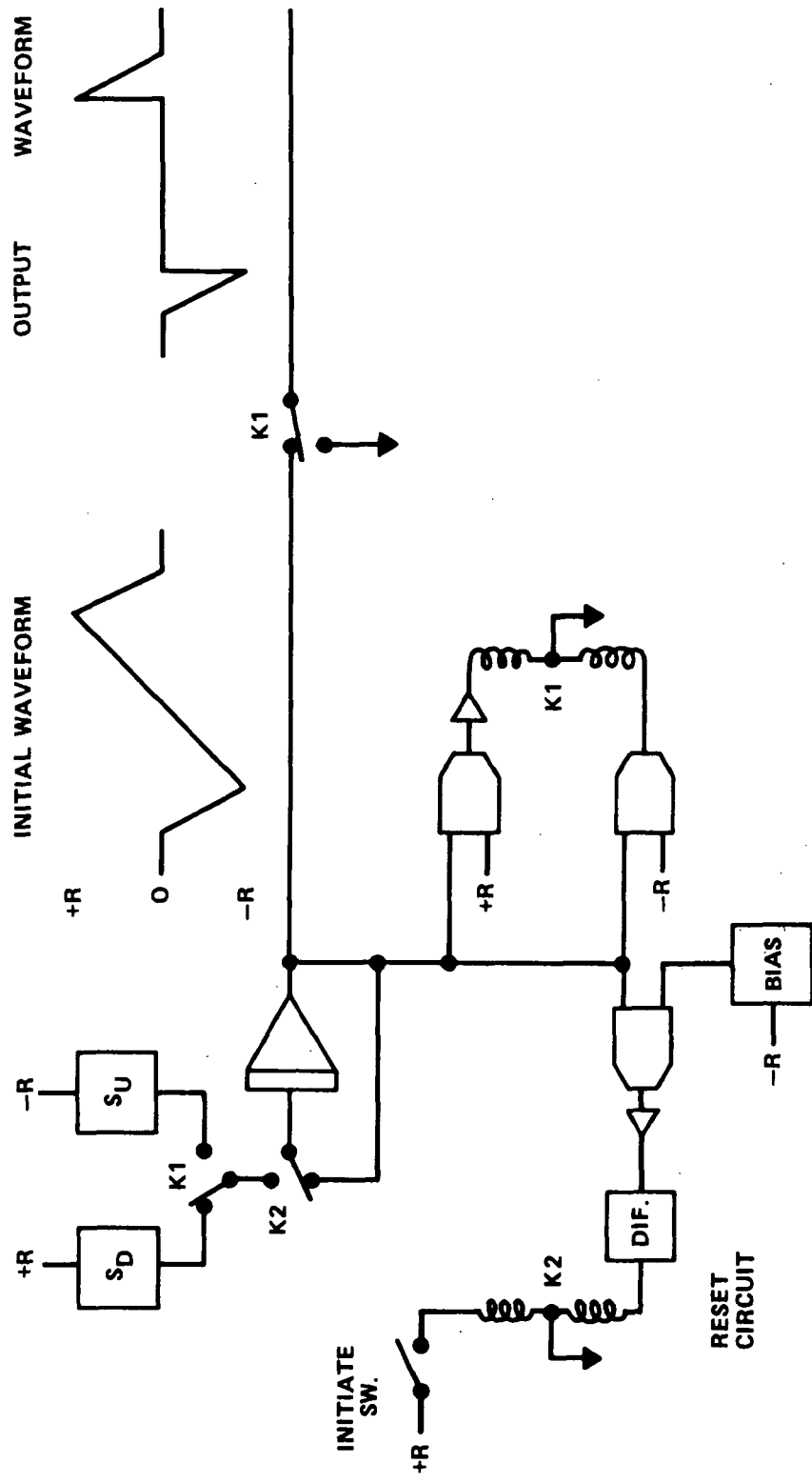
Figure B2. Wall pushoff generator.
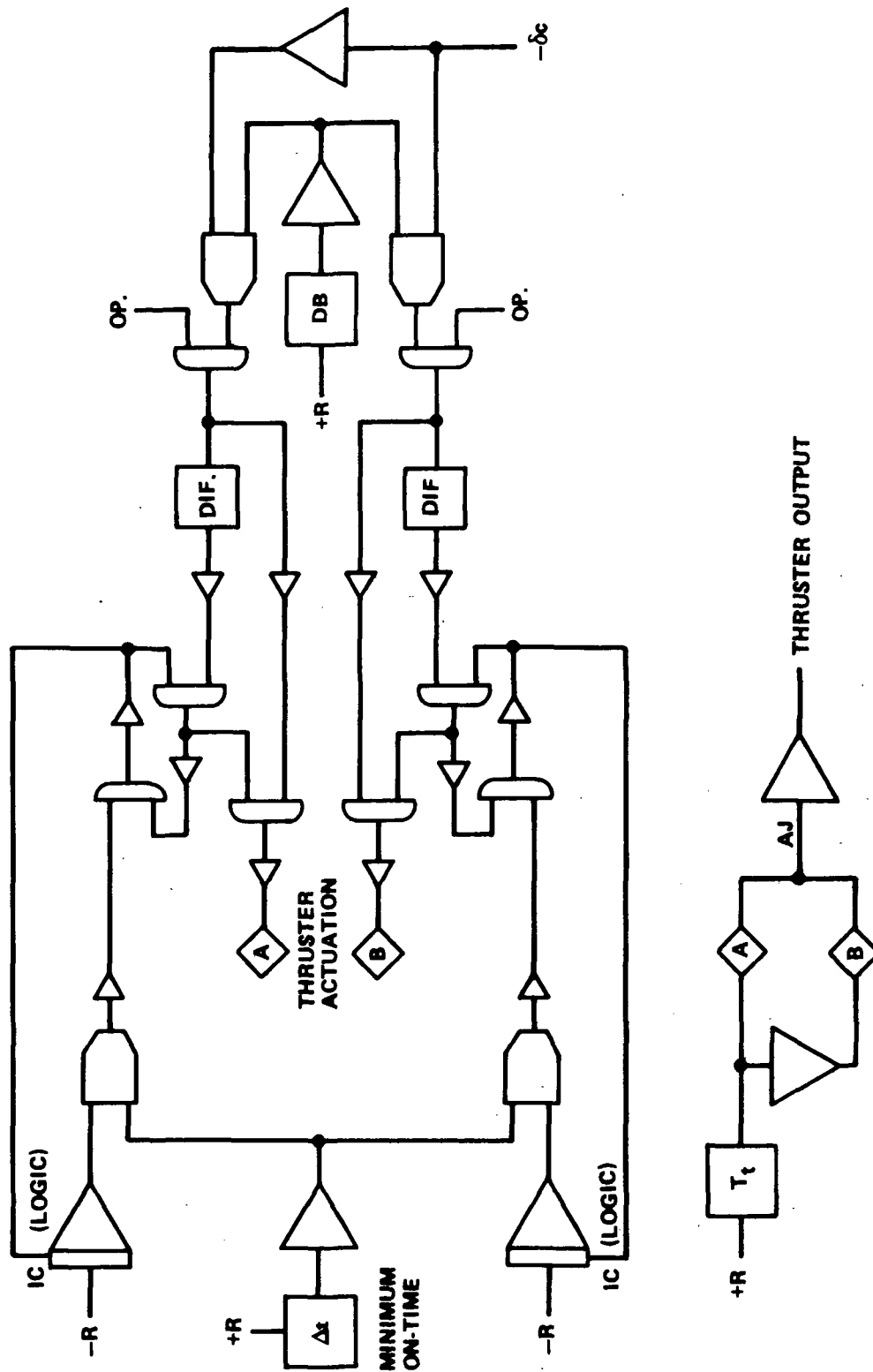
Figure B3.   Thruster implementation.

22

APPENDIX C

ANALOG COMPUTER OUTPUT

Analog computer output in the form of line recordings is presented in this appendix. Significantly more information and insight into the dynamic behavior of the Shuttle/pallet/SEM system are contained in these data than in the summary given in the main body of the report. Each column contains the output data for an individual computer run. A single parameter is changed between runs to demonstrate sensitivity to that variable. A description of the conditions and a brief discussion of the results for each run are contained in the following discussion.

Figure C1 shows that disturbing torques will be transmitted to the experiment base if there is an experiment package center of mass (CM) offset relative to the gimbal axes. This series of runs assumes a completely rigid pallet and ideal gimbal bearing characteristics. The SEM servoloop is similar to the Skylab experiment pointing system (EPS). It has a bandwidth of about 2.3 Hz. The SEM gimbal axis is located 5 m (16.4 ft) from the Shuttle CM. The disturbing torques originate from 4448 N (1000 lb) thruster firings. All thruster operation for this entire study was assumed to be individual firings (no paired or simultaneous firings). All motion occurs about the small moment of inertia axis (roll).

Figure C2 shows the effect of RCS thrust level on experiment base stability. The equivalent on-time is 0.033 s. The thrusters act on a lever arm of 2.8 m (9.2 ft). A value of 0.03 m (0.1 ft) was selected as a typical experiment CM offset for this and all subsequent cases.

Figure C3 shows experiment base response to variation in thruster on time. A 2224 N (500 lb) thruster was used for these runs. A typical minimum on time of 0.033 s was selected for all subsequent runs.

Figure C4 shows the effect of a flexible pallet between the Shuttle and SEM. The rigid pallet case is repeated in the first run to emphasize the attenuation and energy absorption characteristics of the pallet. An internal damping coefficient of about 0.05 is assumed for the pallet structure. A nominal spring constant of 387.7 N-m/arc min is chosen for all subsequent fixed pallet cases.

Figure C5 illustrates the influence of non-ideal gimbal characteristics in transmitting disturbances to the experiment base. The nominal Shuttle/pallet operational characteristics are retained as a disturbing function and spring tension is added across the pallet/SEM gimbal. This is equivalent to a flex pivot or cables with pure spring torques. The effect is to create a linear deflection of the experiment base. The spring deflects as the Shuttle limit cycles within the ±0.5 deg deadband and the SEM position servo develops an "error" proportional to the spring torque. The third case has both spring torque and coulomb friction. This characteristic can result from rolling friction, cable distortion, or magnetic hysteresis in torquers. The effect is to create a steady state torque (and therefore a deflection) because of relative rate about the gimbal point. The fourth case has 2.5 N-m (1.8 ft-lb) of stiction added to the other bearing characteristics. Stiction is an even more detrimental condition than is indicated in this run because actual magnitudes may be four times greater than this for large bearings. The final column is an expanded time base run which shows the detailed response of a non-ideal SEM to a thruster firing.

In Figure C6, additional disturbance functions are introduced into the simulation. The first run is a repeat of the non-ideal SEM case. The effect of signal noise in the SEM control loop is shown in the second run. Random disturbances to the Shuttle such as men involved in routine tasks or operation of machinery is added to the third run and a wall pushoff is superimposed on the other disturbances following the second thruster firing.

Figure C7 illustrates how servoloop characteristics effect experiment base stability. The first column is a repeat of the previous run with all non-ideal gimbal characteristics and disturbance conditions included. The second column represents twice the static gain (40 percent increase in bandwidth) of the Skylab EPS. These gain changes are made to demonstrate the effect on the servoloop and do not represent a design optimization or recommendation for an SEM controller. The third column represents twice the dynamic gain of the Skylab EPS. The fourth column shows the influence of an integral control loop on SEM response.

Figure C8 describes Shuttle and SEM response to gravity gradient torques during one half of an orbit. The Shuttle holds an inertial orientation with 4448 N (1000 lb) thrusters operating to maintain a ±0.5 deg deadband. The run begins without integral control.

Stiction is removed about half way through the run. Integral control is reintroduced during the last quarter of the run. The expanded time scale shows the detailed dynamic behavior of the SEM during a thruster firing and a wall pushoff.

Figure C9 is essentially a repeat of the preceding case with 111 N (25 lb) thrusters operating in a deadband of ±0.1 deg. This case produces unidirectional thruster firings during each quarter orbit in response to gravity gradient torques. This is in contrast to the previous case in which the large thrusters operated almost exclusively in a limit cycle mode. Careful inspection of the Shuttle angular acceleration trace of the expanded time run will show that the wall pushoff resulted in about 1.6 s of continuous thruster operation followed by additional firings at recontact with the other wall. This indicates that man motion can lead to inefficient operation of an RCS with a small deadband.

Figure C10 is another half orbit run with control moment gyros (CMGs) instead of thrusters. Three Skylab-type CMGs supply control torque to the pallet in response to Shuttle-based sensors. The CMG/Shuttle loop has a bandwidth of 0.022 Hz. This is about the same as that of the Skylab cluster. An initial rate is introduced at the start of the run to simulate a transfer from a thruster system. The Shuttle maintains a much smaller attitude with CMGs but the experiment angle and rate have not been improved by either the small thrusters or CMGs. This is because the SEM is doing a satisfactory job of isolating the experiment results from the nonlinear bearing characteristics of stiction and coulomb friction. The frequency of SEM disturbances are actually less in the case of a large thruster operating constantly in a limit cycle mode than with a CMG system which has very small but frequent changes in the direction of motion. This should not be interpreted as a general rule since the results depend on SEM geometry, magnitude of bearing characteristics, and the nature of the disturbing torques.

Figure C11 shows two typical experiment-produced disturbances that are expected for Skylab. The nature of the disturbing function is defined in Reference 4. Although the magnitude of the disturbance is small, it appears directly on the experiment package. The effect on the SEM is evident from the experiment rate and angle.

Figure C12 shows the results from an experiment pointing concept which is entirely different from the SEM. In all the following runs,

the SEM is removed from the simulation and experiment stability is referenced to the pallet, as if the experiments were hard mounted. These runs demonstrate that pallet stability is only slightly improved by adding CMG units. The control gains remain constant; therefore, system bandwidth is only slightly changed. The 3-CMG case has a bandwidth of about 0.022 Hz. Pallet stiffness is the nominal 387.7 N-m/ arc min. There are no gravity gradient, noise, or random torque disturbances. A wall pushoff provides the excitation. Sensor signals are derived from the Shuttle and CMG torque is applied directly to the pallet. The high frequency content of these traces results from the flexibility between sensors and actuators (CMGs).

Figure 13 illustrates the effect of increasing bandwidth to improve stability. The conditions for the previous run remain in effect. This and all subsequent runs are made with three CMG units. Experiment rate and angle are decreased somewhat but only by high control torque requirements. The CMGs go into saturation when bandwidth is increased to about 0.2 Hz.

In Figure C14 the first two runs are made at 0.2 Hz and the dynamic gain is parameterized in an attempt to alleviate CMG saturation. In the last four runs bandwidth is reduced to 0.14 Hz and dynamic gain is increased to improve experiment stability. All cases are constrained by a stability boundary that is established by the flexibility between sensors and actuators.

Figure C15 presents a case where pallet-mounted sensors are used instead of Shuttle sensors. The pallet is now the controlled element and the Shuttle acts as a passive, spring-connected mass. There is no longer a stability limit set by flexibility between Shuttle and pallet. Bandwidth is increased to 4 Hz without encountering a stability boundary. However, this does put the CMGs into saturation because Shuttle oscillation produces large disturbing torques on the pallet. The obvious approach is now to decouple or isolate the pallet as much as possible from direct disturbances by the Shuttle.

In Figure C16, the pallet is attached to the Shuttle with springs and stiffness is changed between runs. The first is made with spring stiffness of 200 N-m/arc min which is less than half the stiffness of the fixed pallet (487.7 N-m/arc min). As the coupling becomes very small, there is a great improvement in pallet and therefore experiment stability. The relative motion between Shuttle and pallet increases

slightly but remains within a reasonable range. The Shuttle motion is now at a very low frequency but sustains because of the very low damping coefficient in the Shuttle/pallet springs.

The first runs in Figure C17 show the level of damping required to prevent long periods of oscillation on the Shuttle. This slightly increases short duration disturbances of the experiments but is beneficial for overall stability. Signal noise and a sample and hold circuit are introduced into the signal lines during the last two runs to check sensitivity to these operational conditions. It is anticipated that as good or better stability can be achieved with this suspended pallet concept at reduced bandwidth by using integral control. There was no attempt to optimize performance or improve capability beyond the indicated level.

Figure C1

28
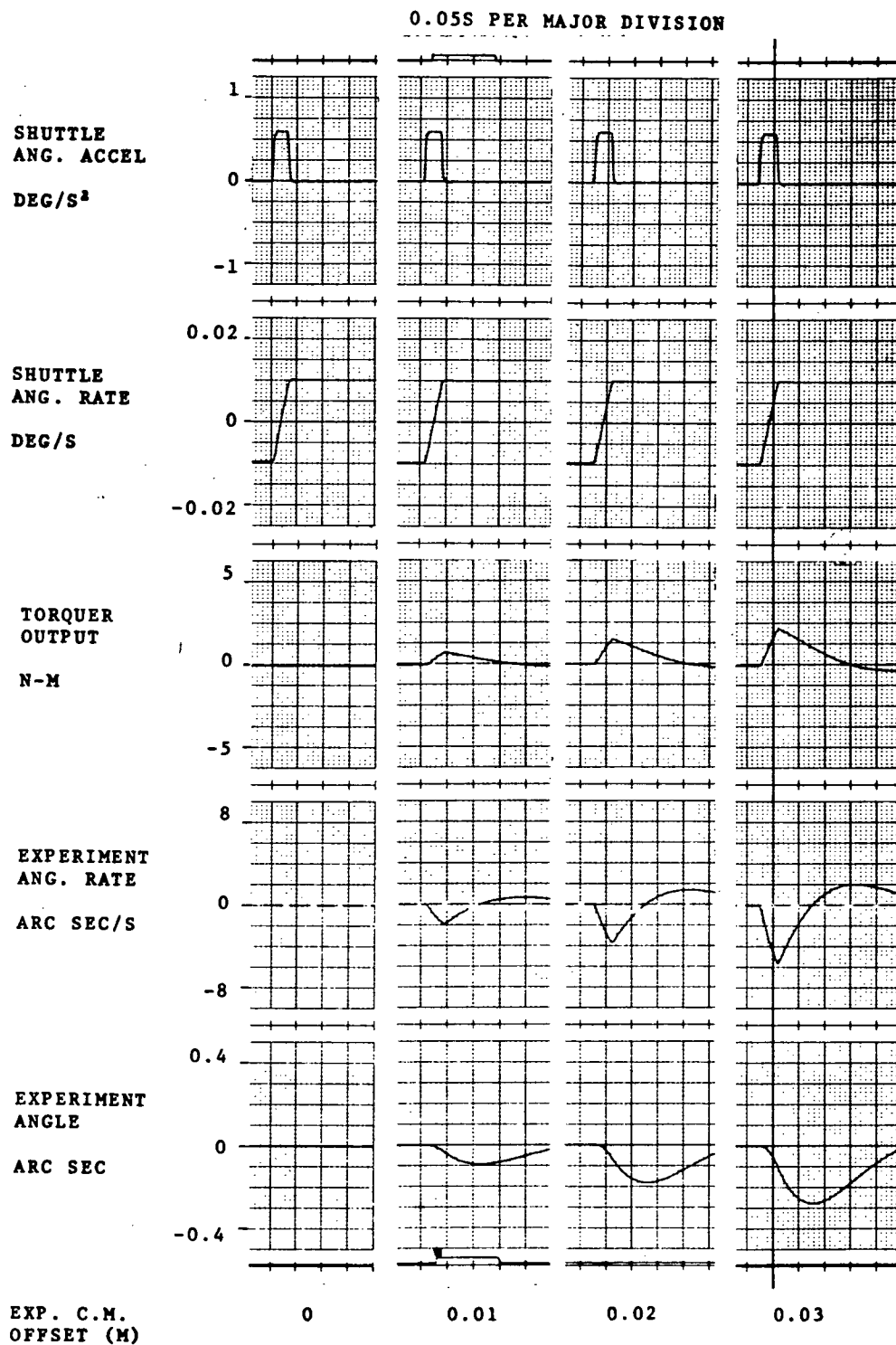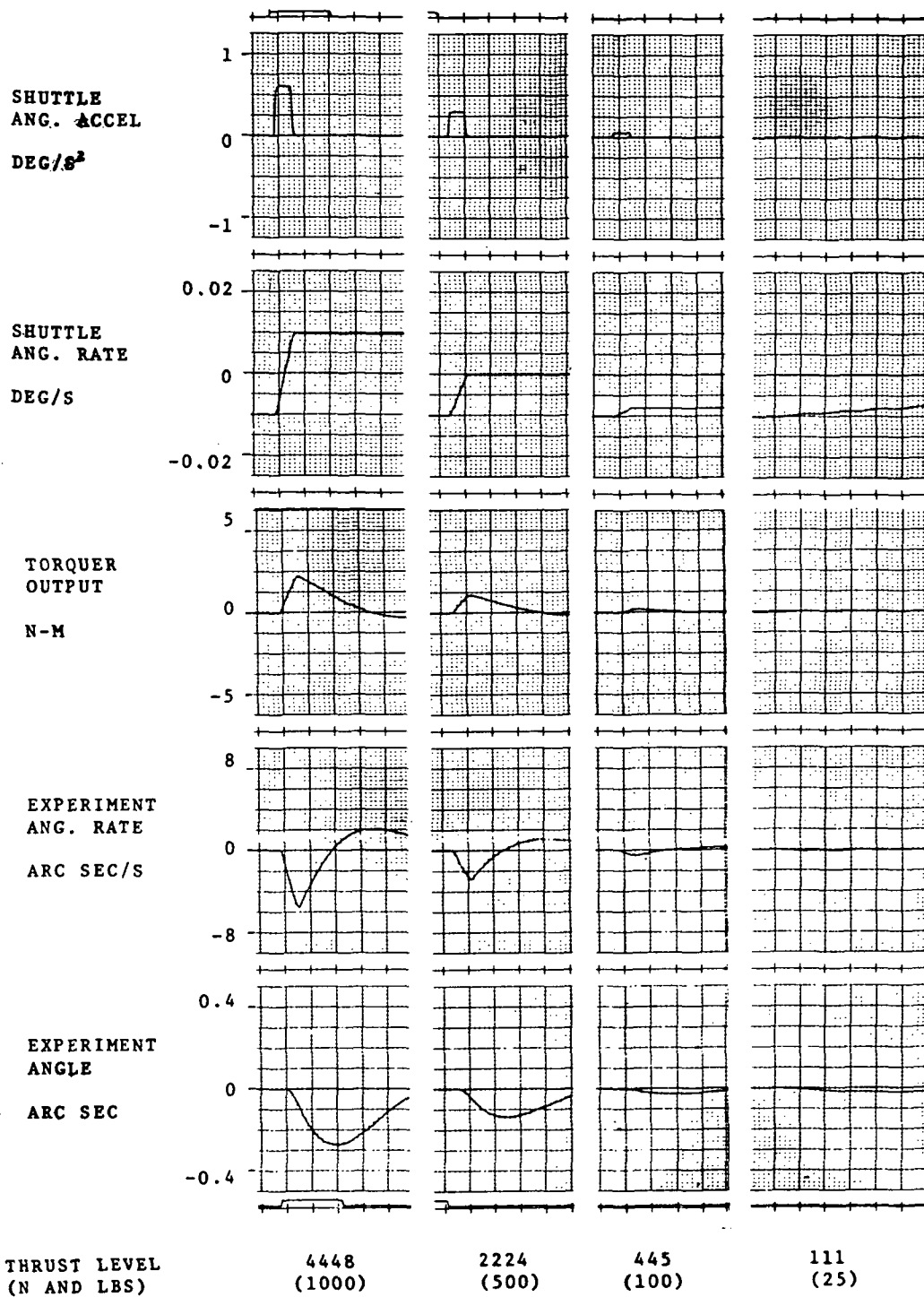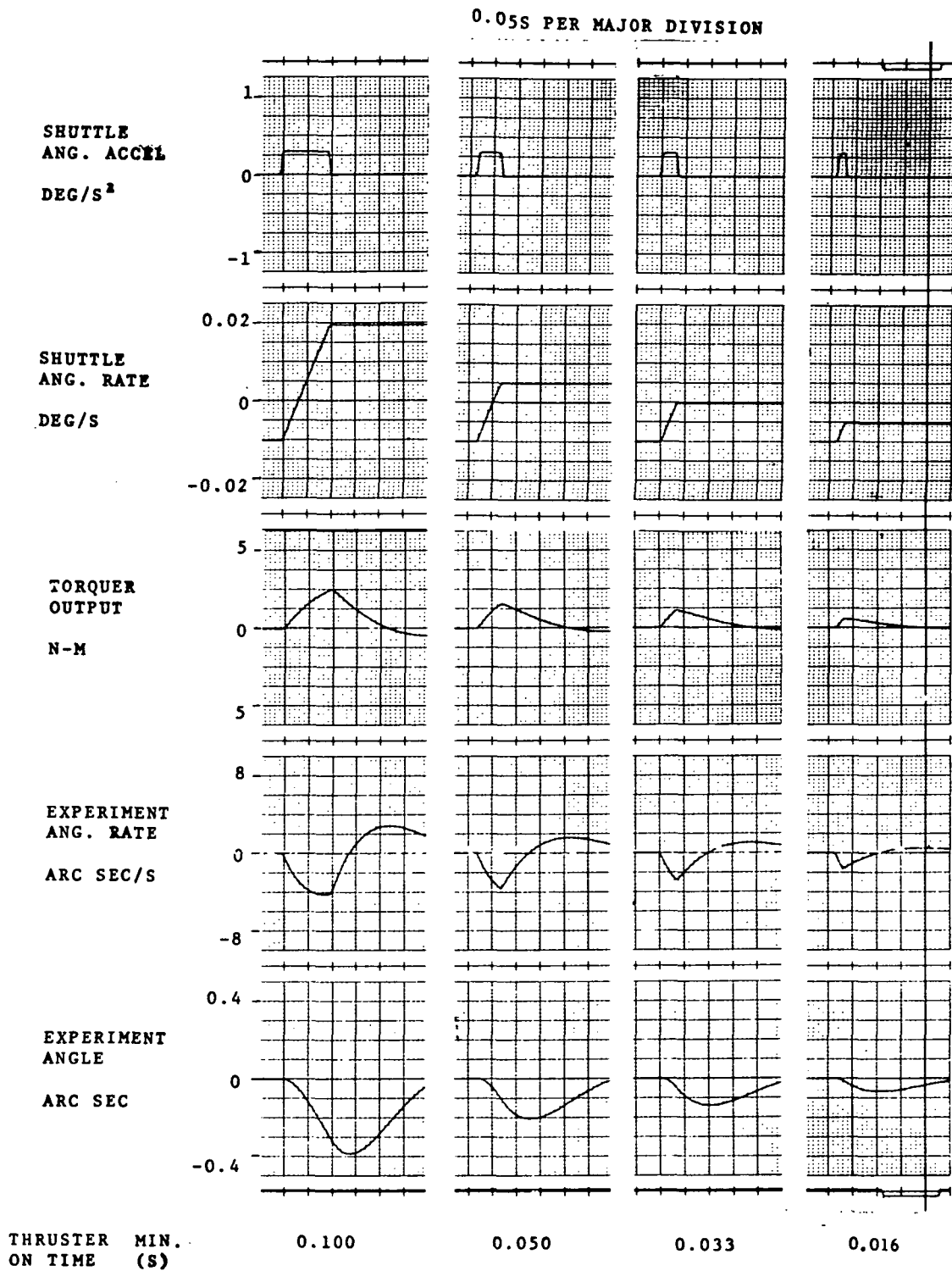
Figure C2

Figure C3
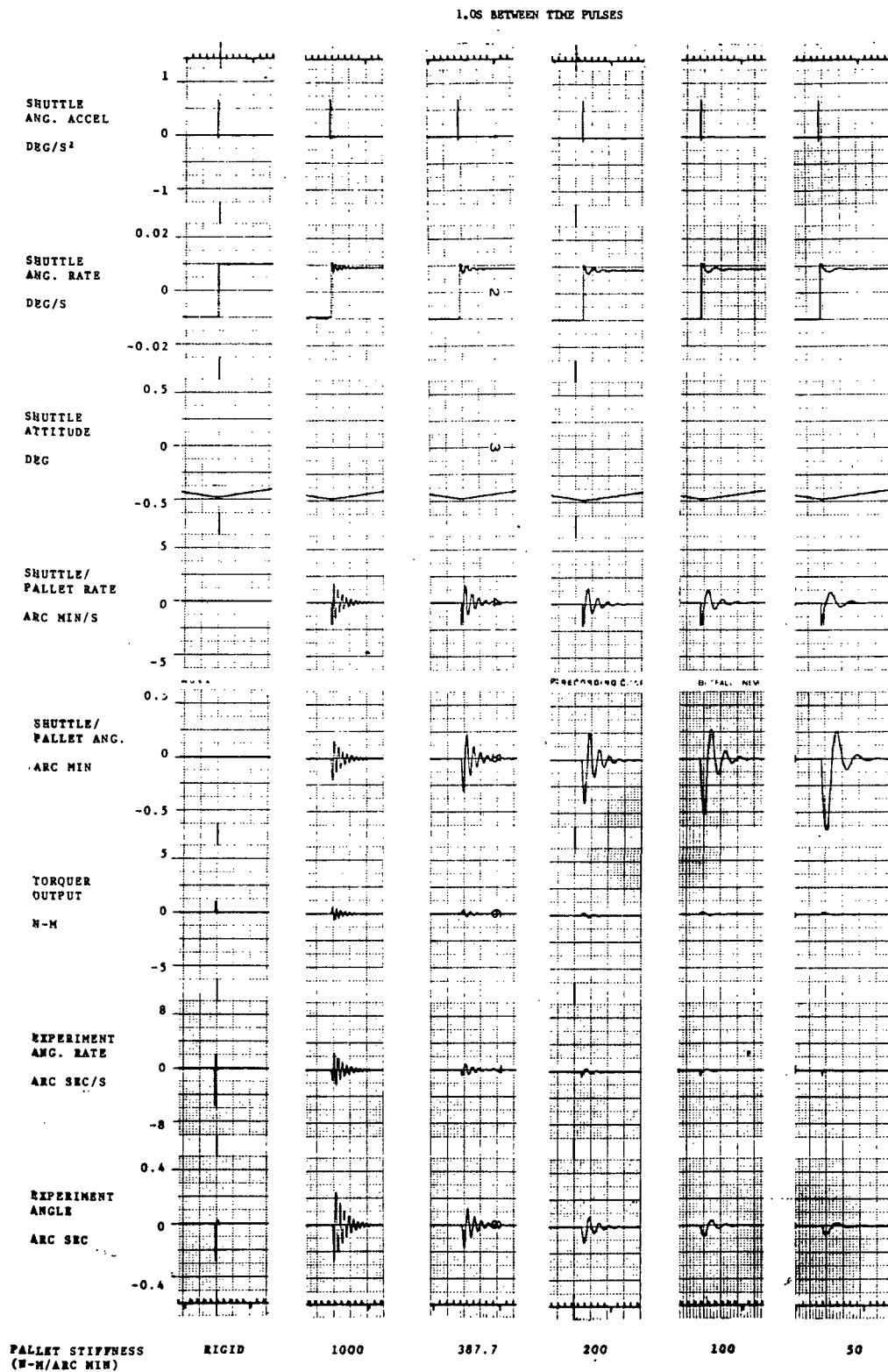
Figure C4
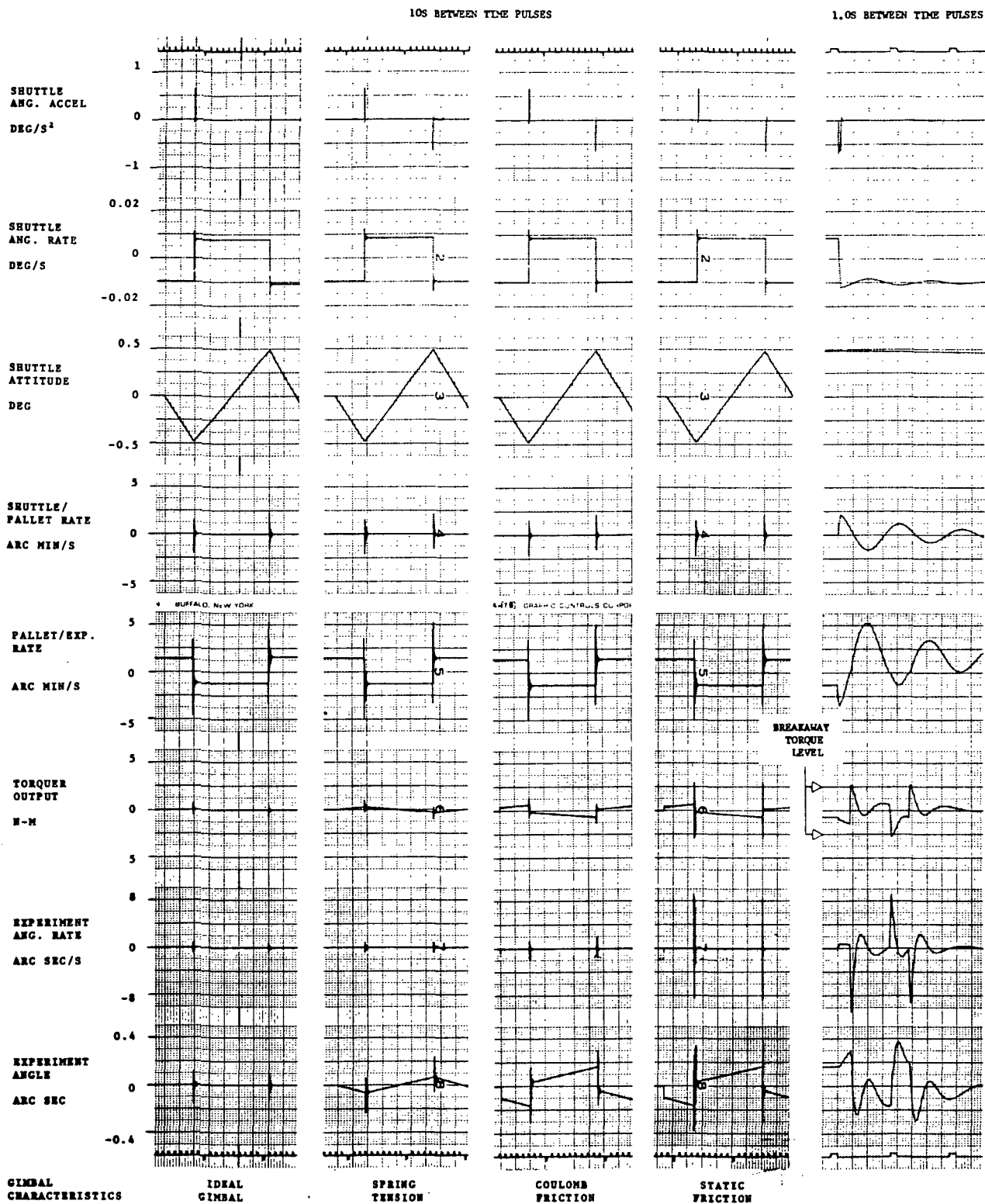
Figure C5
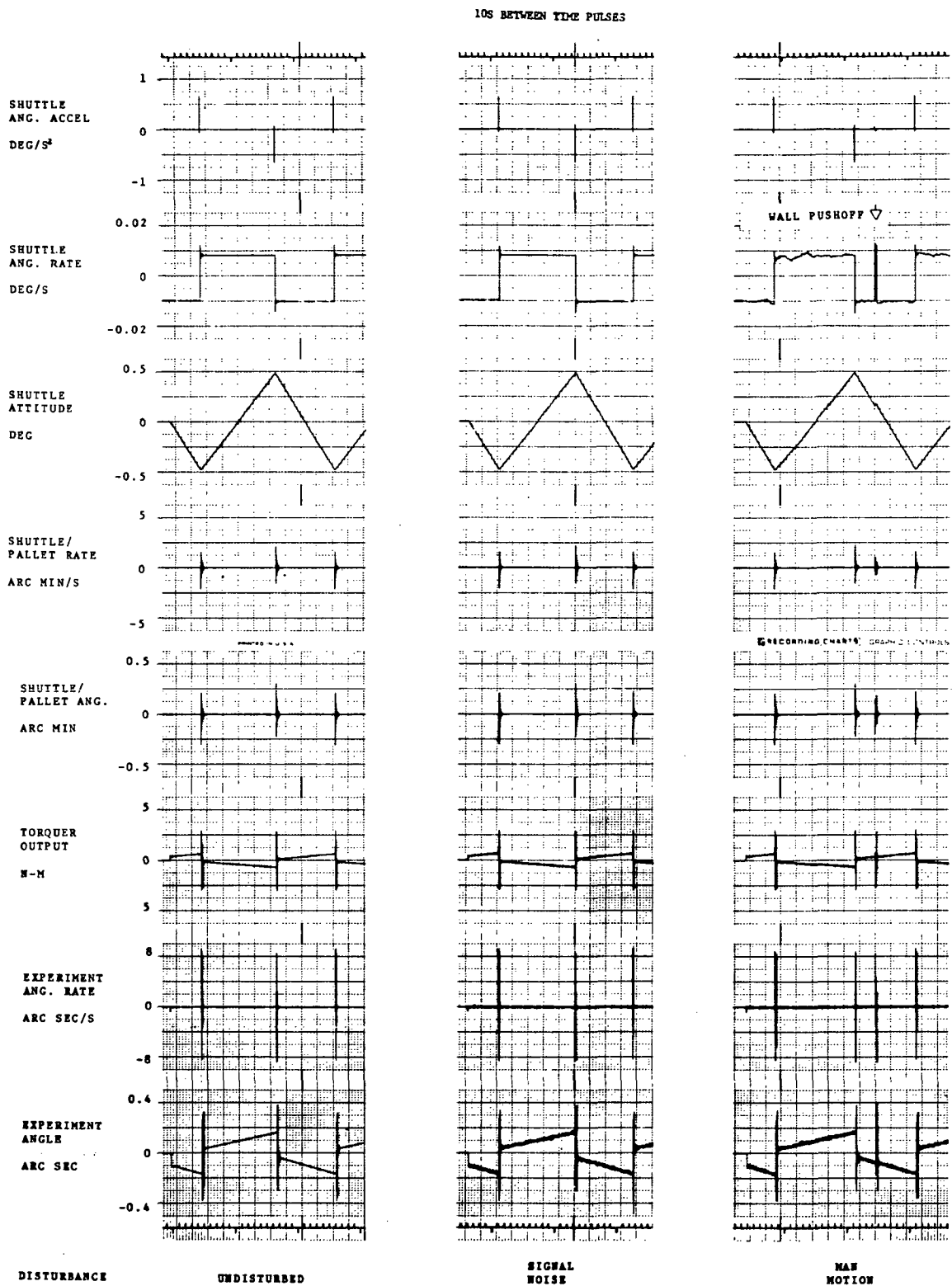
SHUTTLE
ANG. ACCEL

DEG/S²

SHUTTLE
ANG. RATE

DEG/S

SHUTTLE
ATTITUDE

DEG

SHUTTLE/
PALLET RATE

ARC MIN/S

SHUTTLE/
PALLET ANG.

ARC MIN

TORQUER
OUTPUT

N-M

EXPERIMENT
ANG. RATE

ARC SEC/S

EXPERIMENT
ANGLE

ARC SEC

WALL PUSHOFF ⇩

DISTURBANCE   UNDISTURBED   SIGNAL   MAN
                                             NOISE   MOTION

Figure C6

33

Figure C7

34

SHUTTLE
ANG. ACCEL

DEG/S²

SHUTTLE
ANG. RATE

DEG/S

SHUTTLE
ATTITUDE

DEG

SHUTTLE/
PALLET RATE

ARC MIN/S

SHUTTLE/
PALLET ANG.

ARC MIN

TORQUER
OUTPUT

N-M

EXPERIMENT
ANG. RATE

ARC SEC/S

EXPERIMENT
ANGLE

ARC SEC

▽ WALL PUSHOFF

STICTION OUT ▽   ▽ INTEG. CONT. IN

Figure C8

35
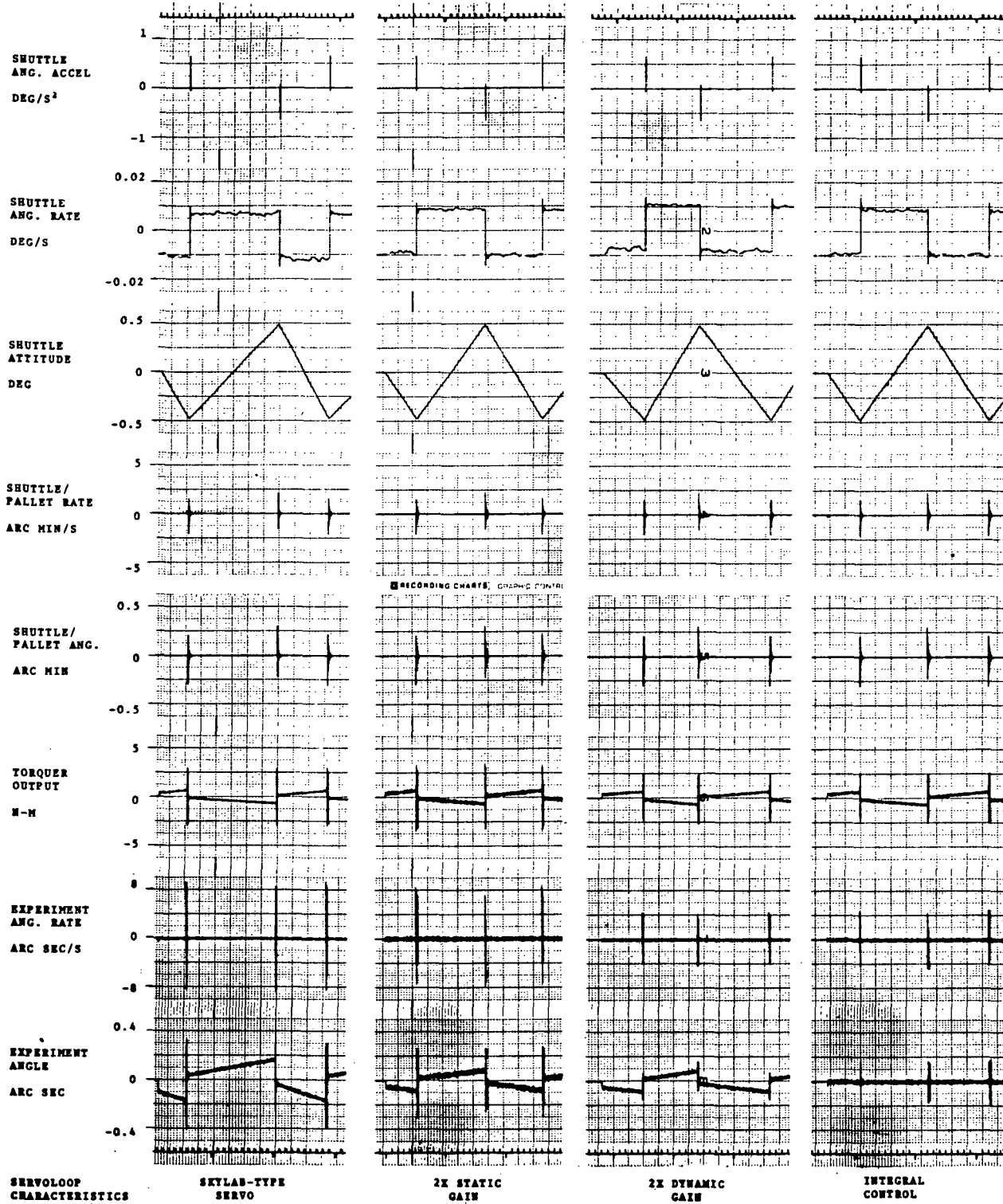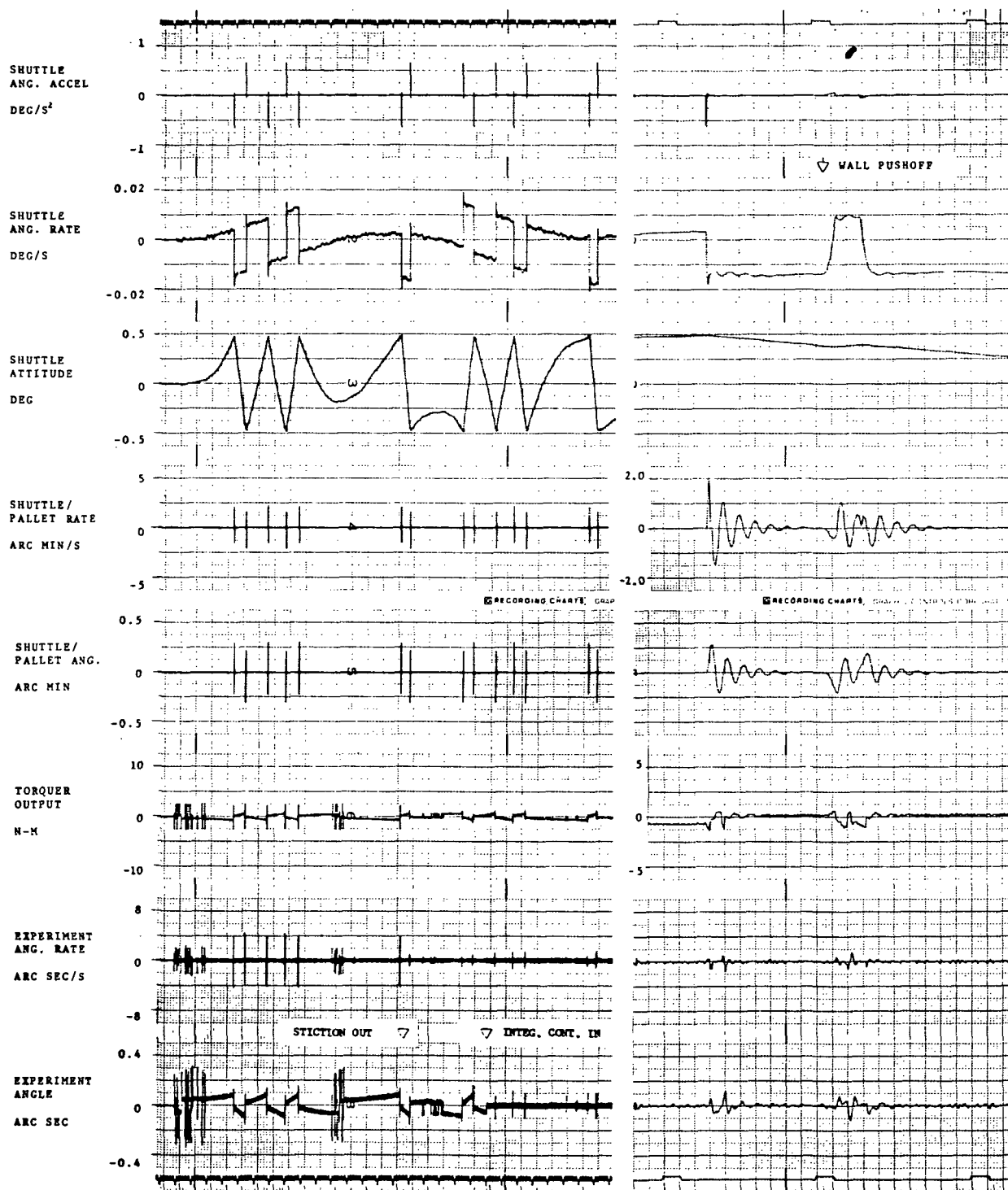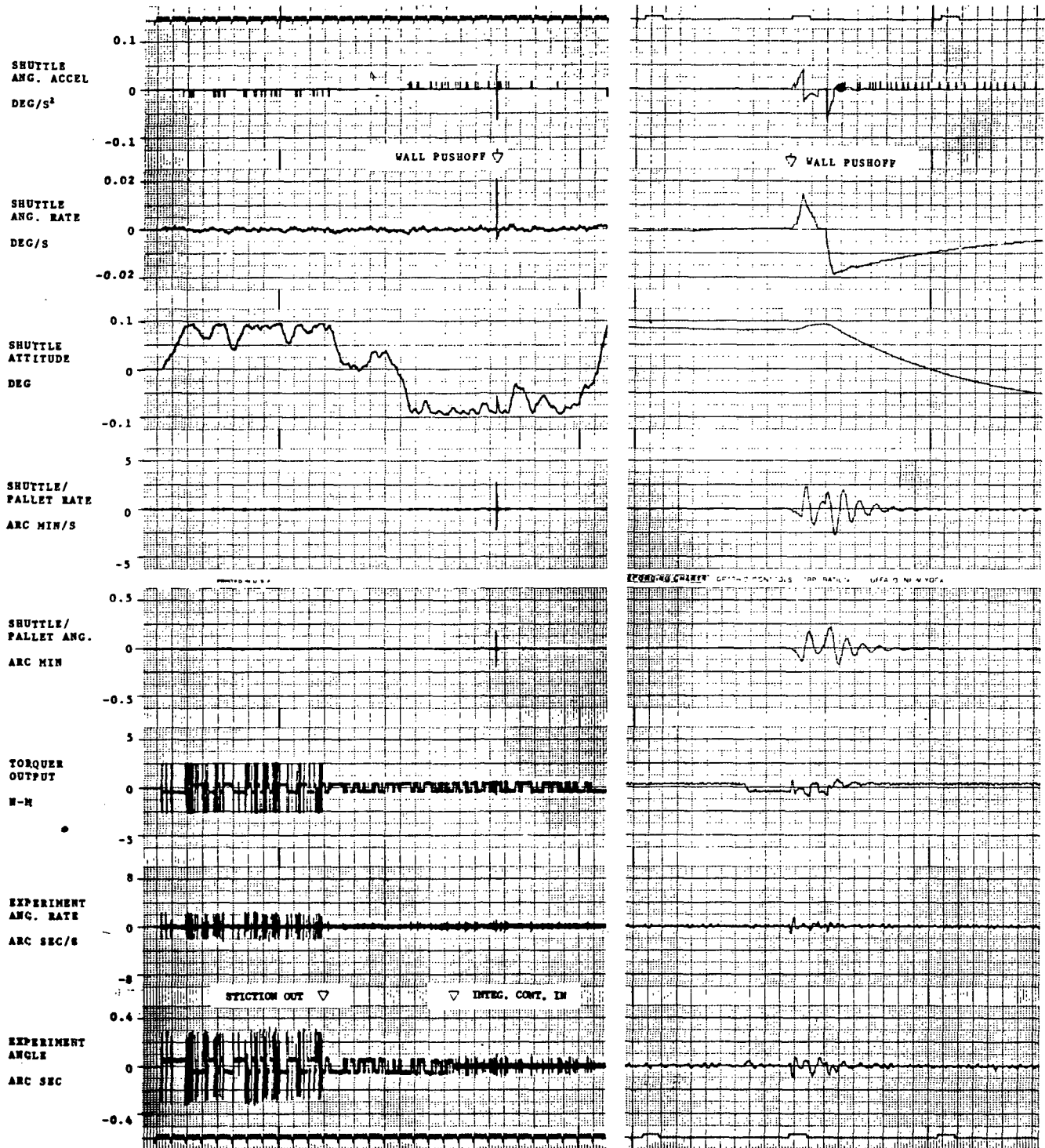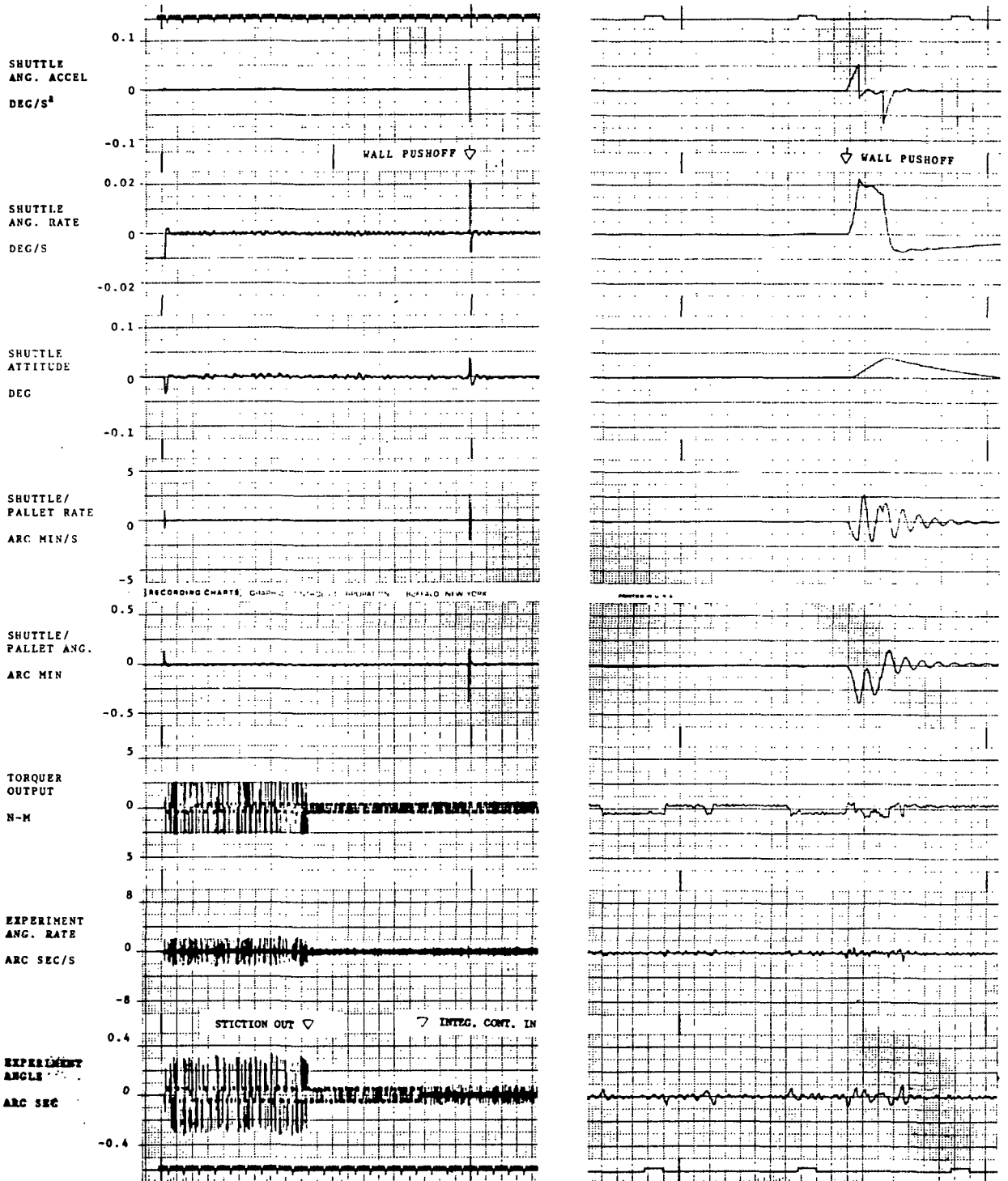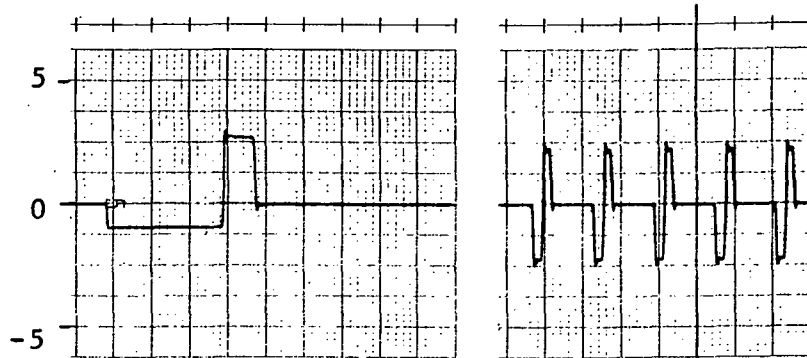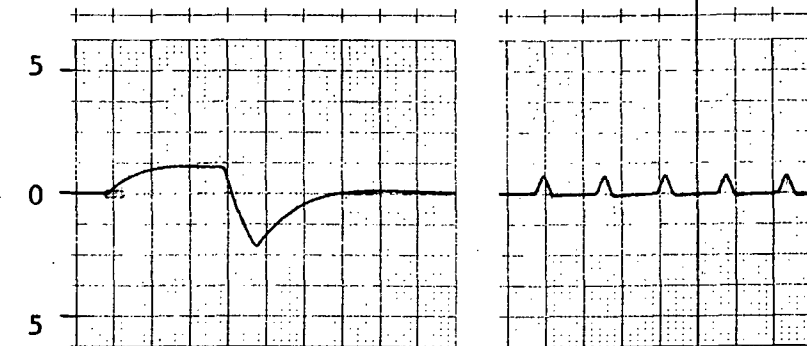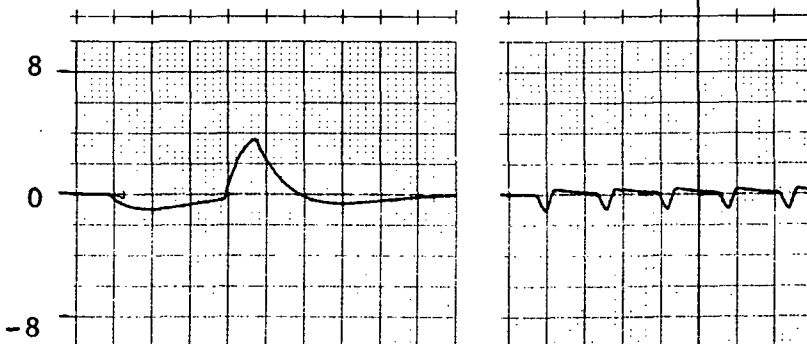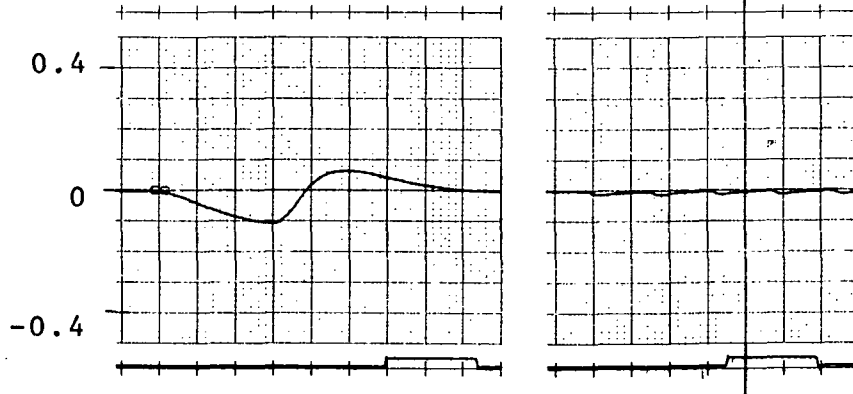
Figure C9

Figure C10
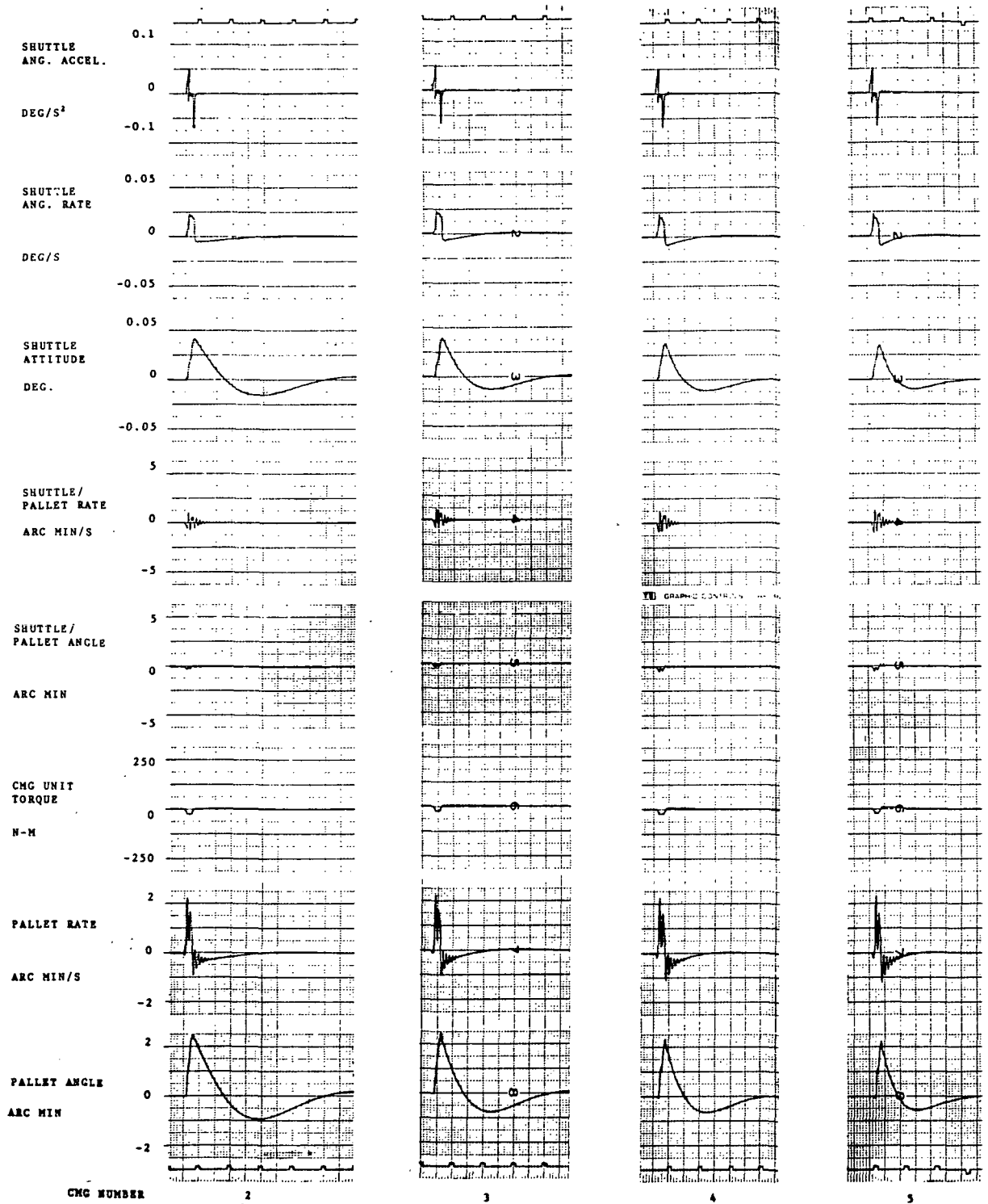
Figure C11

Figure C 12

Figure C 13

Figure C 14

41

Figure C 15

SHUTTLE
ANG. ACCEL.

DEG/S²

SHUTTLE
ANG. RATE

DEG/S

SHUTTLE
ATTITUDE

DEG.

SHUTTLE/PALLET
RATE

ARC MIN/S

SHUTTLE/
PALLET ANGLE

ARC MIN

CMG UNIT
TORQUE

N-M

PALLET RATE

ARC MIN/S

PALLET ANGLE

ARC MIN

PALLET STIFFNESS
(N-M/ARC MIN)

PALLET DAMPING
(N-M/ARC MIN/S)

200	100	50	25
8	6	4	4

Figure C 16

43

Figure C 17

44
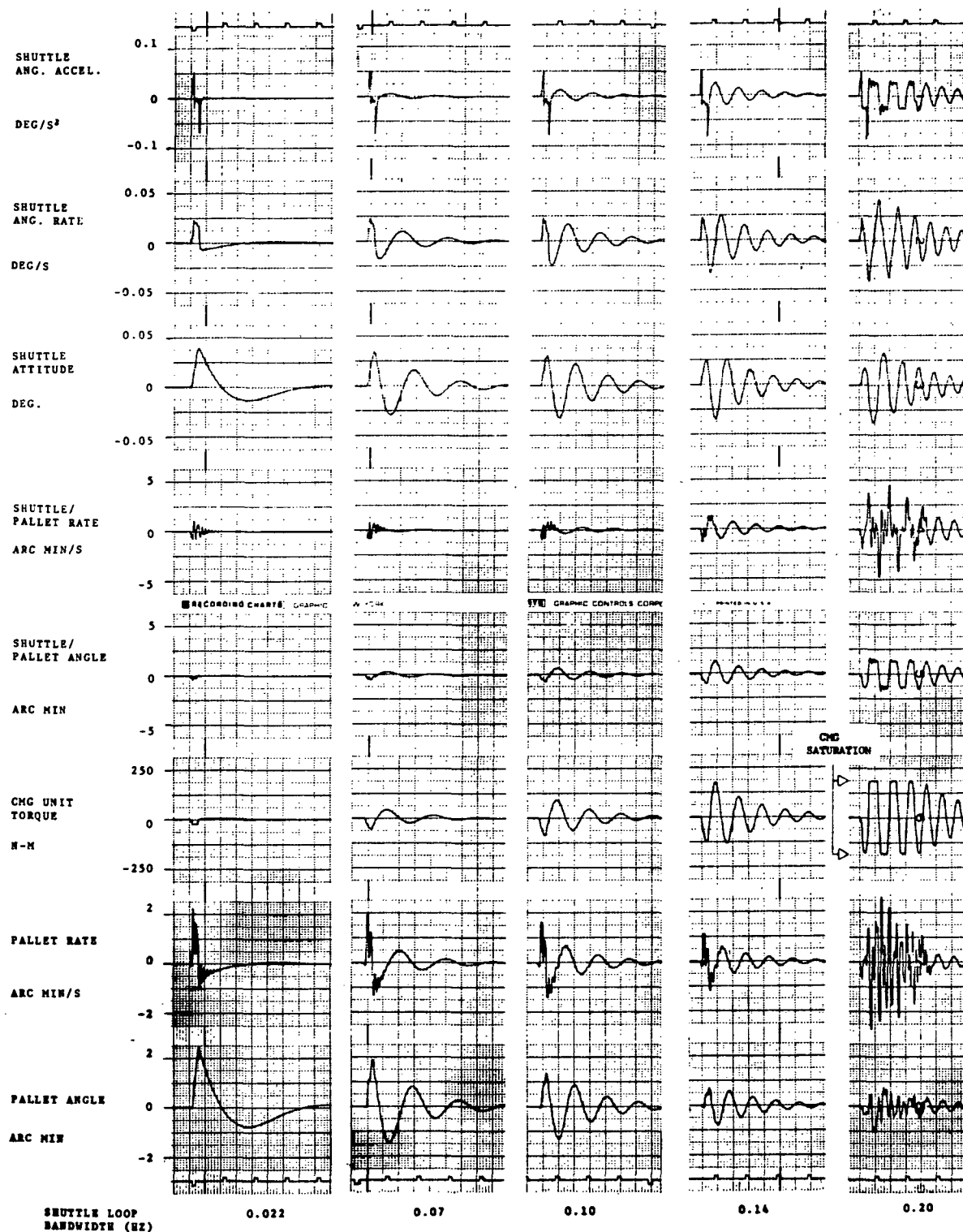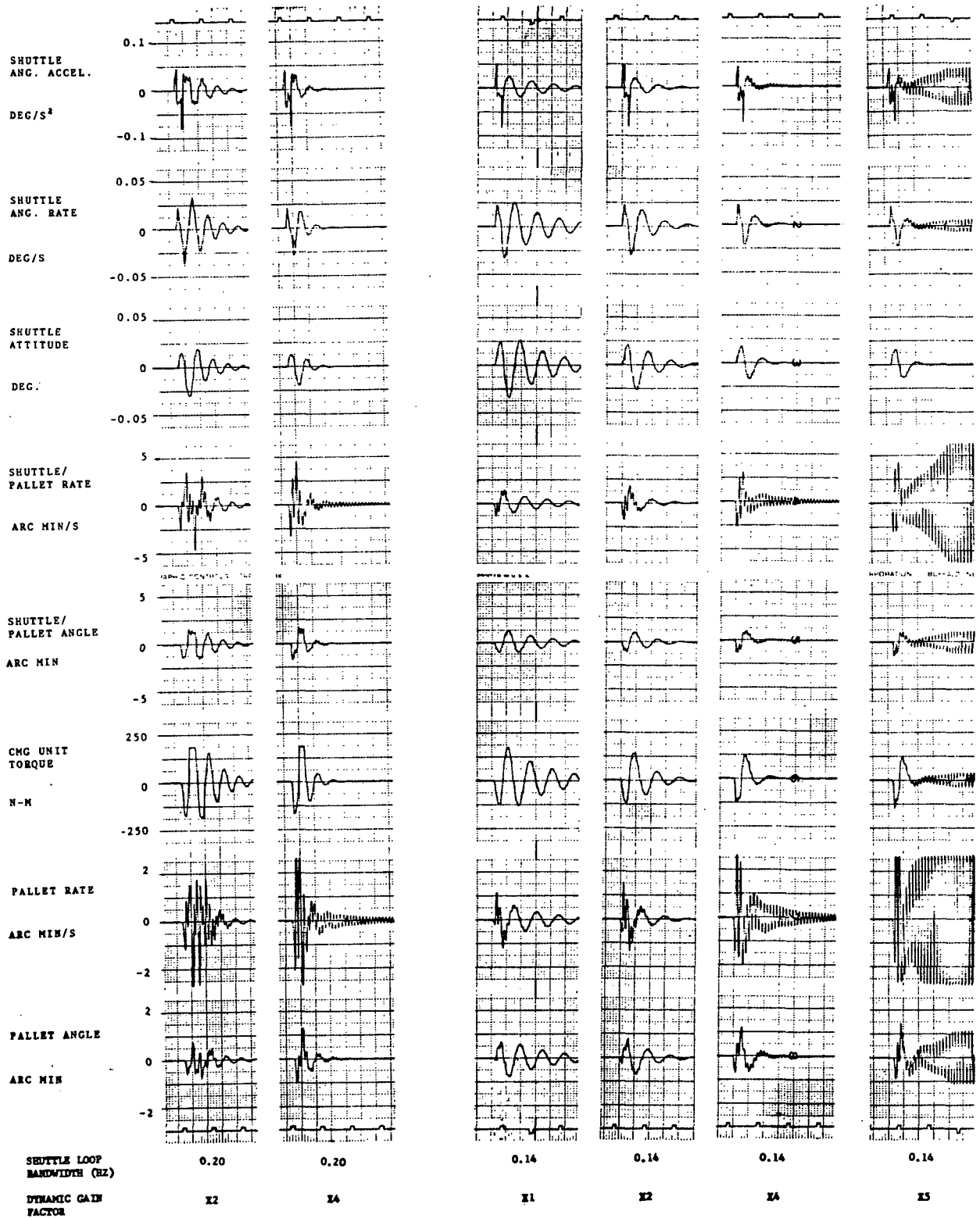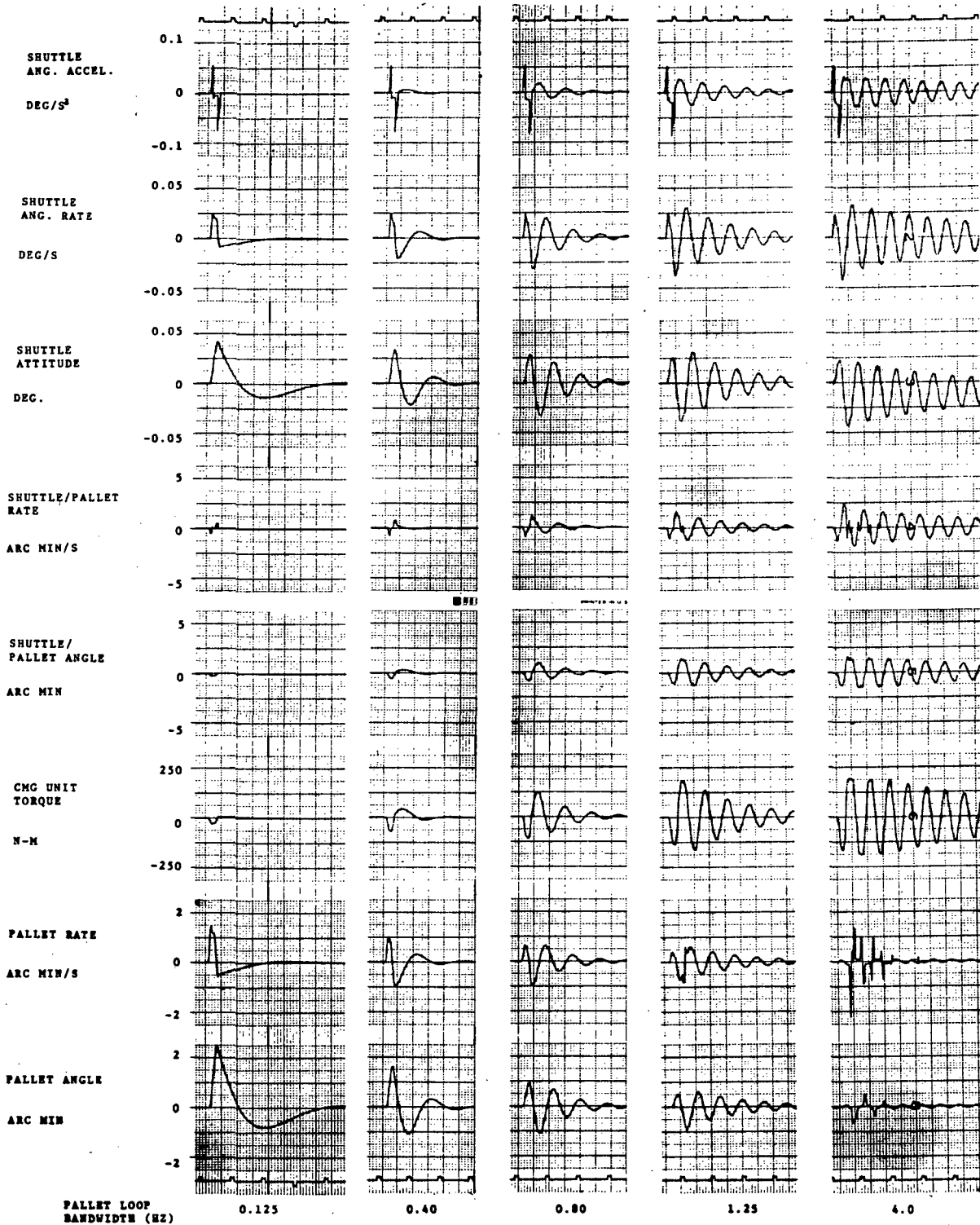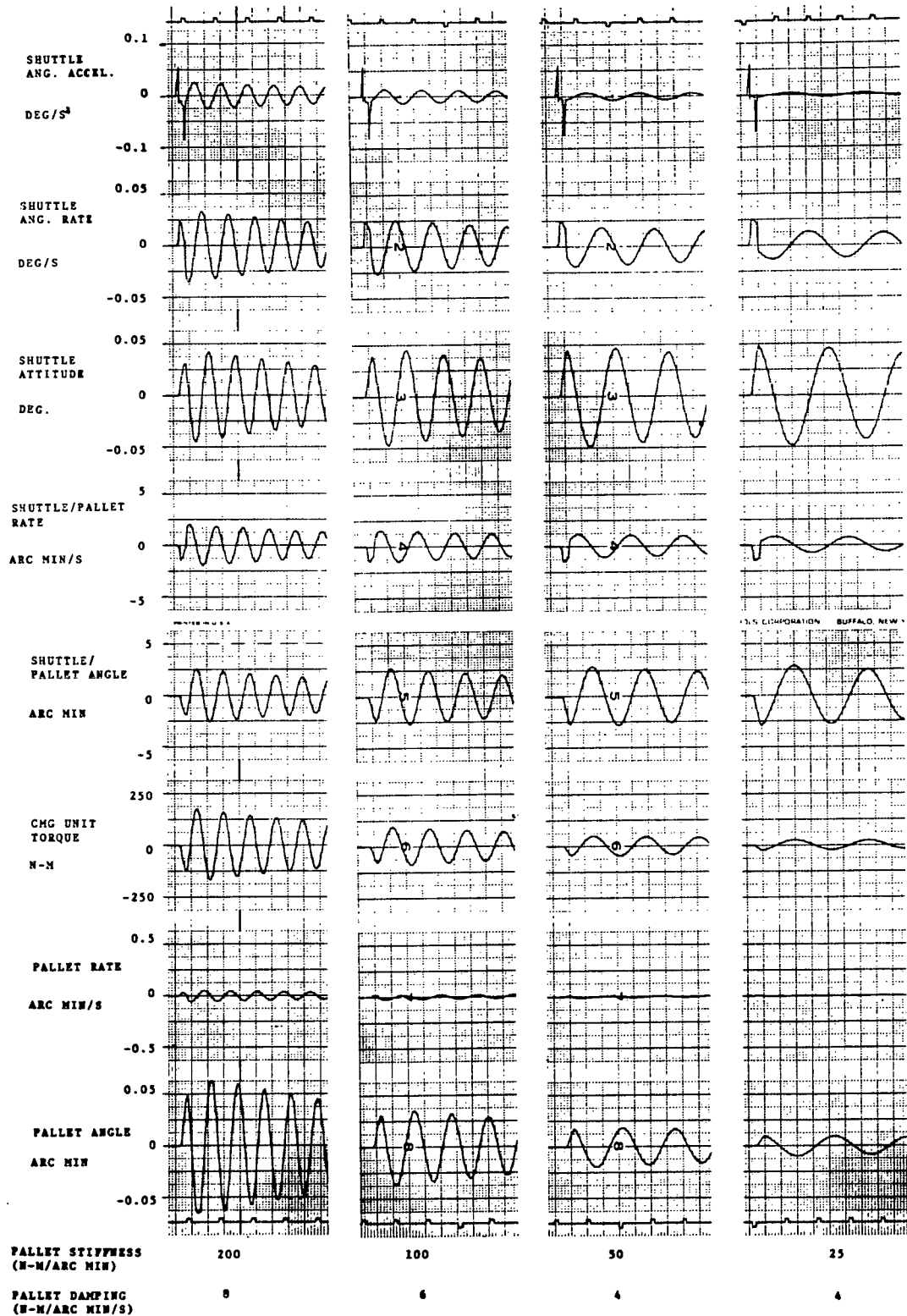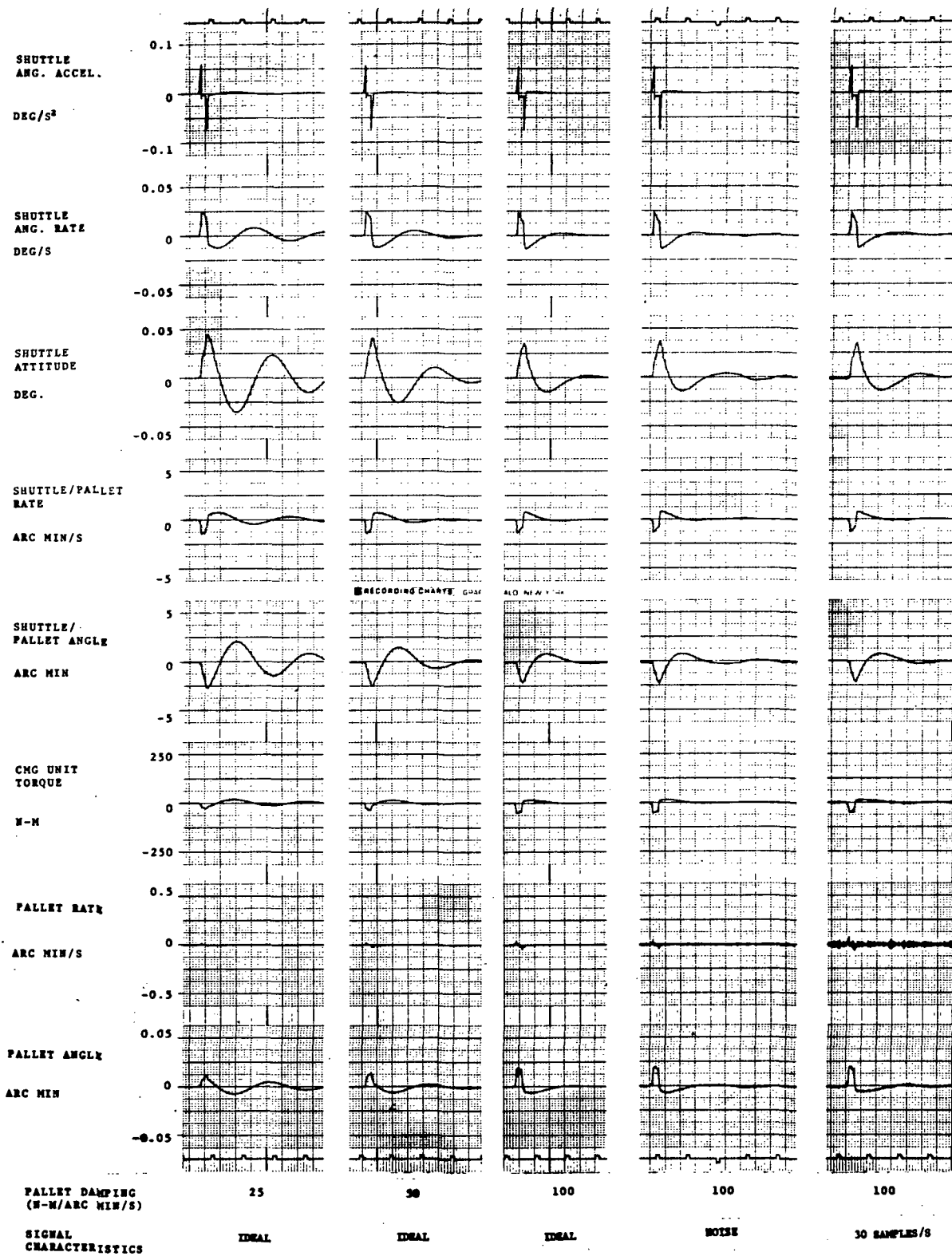
REFERENCES

1. Nicaise, P.D.: Experiment Pointing Control During Space Shuttle Sortie Missions. NASA TM X-64692, January 1972.

2. Shuttle Mass Properties Status Report, Properties Status Report. SD 72-SH-0120-6, North American Rockwell, March 2, 1973.

3. Scofield, Harold N.: Summ ry of Zero "g" Aircraft Crew Motion Experiment. S&E-ASTR-SD-108-70, Sept. 4, 1970.

4. EPC Mass Motion Disturbance Report. ED-2002-1035, Rev. A, The Martin Company, March 2, 1971.

APPROVAL

SIMULATION OF AN EXPERIMENT POINTING SYSTEM
FOR THE SPACE SHUTTLE

By P. D. Nicaise

The information in this report has been reviewed for security classification. Review of any information concerning Department of Defense or Atomic Energy Commission programs has been made by the MSFC Security Classification Officer. This report, in its entirety, has been determined to be unclassified.

This document has also been reviewed and approved for technical accuracy.
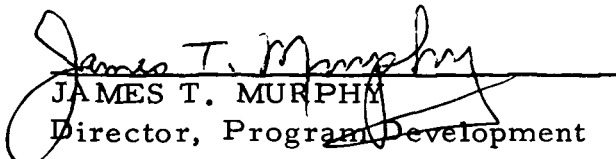
DAVID N. SCHULTZ
Chief, Navigation and Control Systems Branch

FRED E. DIGESU
Chief, Electronics and Control Division

ERICH E. GOERNER
Director, Preliminary Design Office

JAMES T. MURPHY
Director, Program Development

DISTRIBUTION